



**HAL**  
open science

## **Climatology of low-level clouds over Western equatorial Africa based on ground observations and satellites**

Olivier Champagne, R. Aellig, A. Fink, Nathalie Philippon, Pierre Camberlin, Vincent Moron, P. Knippertz, Geneviève Sèze, R. van der Linden

► **To cite this version:**

Olivier Champagne, R. Aellig, A. Fink, Nathalie Philippon, Pierre Camberlin, et al.. Climatology of low-level clouds over Western equatorial Africa based on ground observations and satellites. *Journal of Climate*, 2023, 36 (13), pp.4289-4306. 10.1175/JCLI-D-22-0364.1 . hal-04538960

**HAL Id: hal-04538960**

**<https://hal.science/hal-04538960>**

Submitted on 9 Apr 2024

**HAL** is a multi-disciplinary open access archive for the deposit and dissemination of scientific research documents, whether they are published or not. The documents may come from teaching and research institutions in France or abroad, or from public or private research centers.

L'archive ouverte pluridisciplinaire **HAL**, est destinée au dépôt et à la diffusion de documents scientifiques de niveau recherche, publiés ou non, émanant des établissements d'enseignement et de recherche français ou étrangers, des laboratoires publics ou privés.

# Journal of Climate

## Climatology of low-level clouds over Western equatorial Africa based on ground observations and satellites --Manuscript Draft--

<b>Manuscript Number:</b>	JCLI-D-22-0364
<b>Full Title:</b>	Climatology of low-level clouds over Western equatorial Africa based on ground observations and satellites
<b>Article Type:</b>	Article
<b>Corresponding Author:</b>	Olivier Champagne Université Grenoble Alpes Saint Martin d'Hères, FRANCE
<b>Corresponding Author's Institution:</b>	Université Grenoble Alpes
<b>First Author:</b>	Olivier Champagne
<b>Order of Authors:</b>	Olivier Champagne Raffael Aellig Andreas H. Fink Nathalie Philippon Pierre Camberlin Vincent Moron Peter Knippertz Geneviève Seze Roderick Van Der Linden
<b>Abstract:</b>	<p>The tropical cloud forest ecosystem in Western Equatorial Africa (WEA) is known to be sensitive to the presence of an extensive and persistent low-level stratiform cloud deck during the long dry season from June to September (JJAS). Here we present a new climatology of the diurnal cycle of the low-level cloud cover from surface synoptic stations over WEA during JJAS 1971–2019. For the period JJAS 2008–2019, we also utilized estimates of cloudiness from three satellite products, namely the Satellite Application Facility on Support to Nowcasting and Very Short Range Forecasting (SAFNWC) cloud classification, the Day and Night Microphysical Schemes (DMS/NMS) and cross-sections from CALIPSO and CloudSat (2B-GEOPROF-LIDAR). A comparison with surface stations reveals that the NMS at night together with SAFNWC at daytime yield the smallest biases and highest Heidke skill scores. The climatological analysis reveals that low-level clouds persist during the day over the coastal plains and windward side of the low mountain ranges. Conversely, on their leeward sides, i.e. over the plateaus, a decrease of the low-level cloud frequency is observed in the afternoon, together with a change from stratocumulus to cumulus. At night, the low-level cloud deck reforms quickly over this region with the largest cloud occurrence frequencies in the morning. Vertical profiles from 2B-GEOPROF-LIDAR reveal cloud tops below 3000 m even at daytime. The station data and the suitable satellite products form the basis to better understand the physical processes controlling the clouds and to evaluate cloudiness from reanalyses and models.</p>

1 **Climatology of low-level clouds over Western equatorial Africa based on**  
2 **ground observations and satellites**

3  
4 O. Champagne<sup>a</sup>, R. Aellig<sup>b</sup>, A. H. Fink<sup>b</sup>, N. Philippon<sup>a</sup>, P. Camberlin<sup>c</sup>, V. Moron<sup>d</sup>, P.  
5 Knippertz<sup>b</sup>, G. Seze<sup>e</sup>, and R. van der Linden<sup>b</sup>

6 <sup>a</sup> *Institut des Géosciences de l'Environnement, Université Grenoble Alpes, CNRS, Grenoble, France*

7 <sup>b</sup> *Institute of Meteorology and Climate Research, Karlsruhe Institute of Technology, Karlsruhe, Germany*

8 <sup>c</sup> *Centre de Recherches de Climatologie, UMR 6282 Biogéosciences, CNRS/Université de Bourgogne Franche-*  
9 *Comté, Dijon, France*

10 <sup>d</sup> *Aix Marseille Univ, CNRS, IRD, INRA, Coll France, CEREGE, F-13000 Aix-en-Provence, France*

11 <sup>e</sup> *LMD, IPSL, UPMC, CNRS, EP, ENS, 4 place Jussieu, F-75000 Paris, France*

12  
13 *Corresponding author: Olivier Champagne, [olivier.champagne@univ-grenoble-alpes.fr](mailto:olivier.champagne@univ-grenoble-alpes.fr)*  
14

## ABSTRACT

15

16 The tropical cloud forest ecosystem in Western Equatorial Africa (WEA) is known to be  
17 sensitive to the presence of an extensive and persistent low-level stratiform cloud deck during  
18 the long dry season from June to September (JJAS). Here we present a new climatology of  
19 the diurnal cycle of the low-level cloud cover from surface synoptic stations over WEA  
20 during JJAS 1971–2019. For the period JJAS 2008–2019, we also utilized estimates of  
21 cloudiness from three satellite products, namely the Satellite Application Facility on Support  
22 to Nowcasting and Very Short Range Forecasting (SAFNWC) cloud classification, the Day  
23 and Night Microphysical Schemes (DMS/NMS) and cross-sections from CALIPSO and  
24 CloudSat (2B-GEOPROF-LIDAR). A comparison with surface stations reveals that the NMS  
25 at night together with SAFNWC at daytime yield the smallest biases and highest Heidke skill  
26 scores. The climatological analysis reveals that low-level clouds persist during the day over  
27 the coastal plains and windward side of the low mountain ranges. Conversely, on their  
28 leeward sides, i.e. over the plateaus, a decrease of the low-level cloud frequency is observed  
29 in the afternoon, together with a change from stratocumulus to cumulus. At night, the low-  
30 level cloud deck reforms quickly over this region with the largest cloud occurrence  
31 frequencies in the morning. Vertical profiles from 2B-GEOPROF-LIDAR reveal cloud tops  
32 below 3000 m even at daytime. The station data and the suitable satellite products form the  
33 basis to better understand the physical processes controlling the clouds and to evaluated  
34 cloudiness from reanalyses and models.

## 35 1. Introduction

36 Many tropical wet forest ecosystems are tightly linked to the presence of low-level  
37 clouds. These clouds reduce water demand and favor photosynthesis by enhancing diffuse  
38 radiation (Karger et al. 2021), and in montane cloud forests they result in ‘hidden’  
39 precipitation through leaf wetting (Berry and Goldsmith 2020; Goldsmith et al. 2013).  
40 Western Equatorial Africa (WEA), encompasses southern Cameroon, Gabon and the  
41 Republic of Congo and comprises the Ogooué and Kioulou-Niari basins as well as the Cristal  
42 and Chaillu Mountains and Batéké plateau (Figure 1). It harbors large expanses of dense,  
43 evergreen to semi-evergreen rain forests, whose presence is associated with a very high intra-  
44 annual and inter-annual stability of the cloud cover (Wilson and Jetz 2016). Philippon et al.,  
45 (2019 and 2022) have provided evidence of low solar irradiance and low sunshine duration  
46 levels during the main dry season (June–September, JJAS) due to persistent low-level clouds.

47 Recent studies suggest a potential climate change threat on this forested region (Oliveira et al.  
48 2014), and mainly a drying trend in Gabon (Bush et al. 2020) and an increase in shortwave  
49 radiation further east in the Congo Basin (Burnett et al. 2020). Moreover, the years with very  
50 warm sea surface temperatures in the eastern Atlantic favored less stratiform clouds in Gabon  
51 (Maley and Hilaire 1993). Further back, a strengthening of the El Niño-Southern Oscillation  
52 (ENSO) variability, likely forced the WEA rain forest to retreat 2000 years ago (Bayon et al.,  
53 2019). This past retreat suggests a general vulnerability of this forest to climatic variations.  
54 A potential threat through the ongoing climate change motivates the research on low-level  
55 clouds in this region.

56 Despite these recent climatic trends and the potential high vulnerability of WEA forests  
57 under climate change, very few studies have focused on the low-level clouds in WEA in  
58 contrast to some neighboring regions such as the southeastern tropical and subtropical  
59 Atlantic Ocean (Wood et al., 2012; Painemal et al., 2015), southern West Africa (SWA;  
60 Kalthoff et al. 2018; Knippertz et al. 2011; Lohou et al. 2020; Schrage and Fink 2012;  
61 Schuster et al. 2013; van der Linden et al. 2015) or the Namib desert in southwestern Africa  
62 (Andersen and Cermak 2018; Andersen et al. 2019, 2020). The southeastern tropical and  
63 subtropical Atlantic Ocean is covered by an extensive layer of marine stratus at the low-level  
64 inversion (Wood 2012; Painemal et al. 2015). This is particularly so in boreal summer, when  
65 the coastal upwelling extends northward to Cape Lopez (0°37'S) and the equatorial  
66 upwelling cools the eastern equatorial Atlantic Ocean (Adebiyi and Zuidema 2018; Fuchs et  
67 al. 2018; Hu et al. 2008). In SWA, low-level clouds are mainly present during the JJAS  
68 monsoon season. At night the low-level clouds rapidly expand from the coast inland and peak  
69 in the morning hours covering an area of nearly 800,000 km<sup>2</sup> (van der Linden et al. 2015).  
70 The processes involved in the nighttime genesis and daytime lysis of the low-level clouds  
71 involves a complicated multi-phase balance between cold air advection from the Atlantic  
72 Ocean and divergence of net radiation and turbulent fluxes, partly in association with a  
73 developing nighttime low-level jet (Knippertz et al. 2015; Lohou et al. 2020). On the  
74 contrary, in the Namib region, low-level clouds form over the ocean during the night, are  
75 advected to the land, and dissipate quickly in the morning (Andersen et al. 2020).

76 While the relative roles of cloud advection from the nearby Atlantic Ocean, orographic  
77 cloud genesis, and boundary layer processes have not been assessed thoroughly for WEA yet,  
78 a first important spatiotemporal climatology of low-level clouds was presented in Dommo et  
79 al. (2018). They used station observations, satellite data, and the European Centre for

80 Medium-Range Weather Forecasts Interim reanalysis (Dee et al. 2011) over WEA to show  
81 that dry season low-level cloud cover is developing in May, peaks in July-August and then  
82 decreases again in October. These clouds tend to be more present in the morning, similarly to  
83 what has been described for SWA (van der Linden et al. 2015). The low-level clouds are  
84 more prevalent in the coastal plains and decrease inland, likely associated with a Foehn effect  
85 leeward of the Chaillu, Cristal Mountains and Batéké Plateau (Fig. 1) leading to dissipation  
86 of the cloud deck associated with the southwesterly to westerly low-level winds. The  
87 formation of low-level clouds could also be favored by biomass burning aerosols that  
88 increase air-mass stability (Solmon et al. 2021; Mallet et al. 2021).

89 Dommo et al. (2018) use the cloud classification from the Satellite Application Facility  
90 on Support to Nowcasting and Very Short Range Forecasting (SAFNWC; (Derrien and Le  
91 Gléau 2005), which has the advantage of a high spatial and temporal resolution and was  
92 previously used to describe daytime low-level clouds in SWA (van der Linden et al., 2015).  
93 However, SAFNWC has difficulties detecting very low-level clouds at night (van der Linden  
94 et al., 2015) and a validation against in-situ synoptic observations was not performed  
95 extensively in Dommo et al. (2018). Thus, the goal of the present study is to complement and  
96 expand on the study by Dommo et al. (2018) In particular, our study relies on an improved  
97 database for in-situ observations of clouds which contains more stations (62) over a longer  
98 period (1971–2019). The spatial sampling is therefore increased, giving a better view of the  
99 low-level clouds cover spatial pattern and conferring robustness to our results. The longer  
100 overlap period between in-situ observations and satellite estimates (2008-2019 against 2008-  
101 2009 in Dommo et al, 2018) enables computing scores of performances, thus quantitatively  
102 evaluating the satellites datasets. In addition, we consider 8 genus of low clouds and not only  
103 the total low clouds cover as in Dommo et al (2018). This allows us to precisely document (i)  
104 the evolution from one genus to another along the diurnal cycle and (ii) how well these  
105 different genera are detected by satellites. Lastly, we worked with (i) day and night  
106 microphysical schemes (NMS/DMS, Lensky and Rosenfeld 2008) giving a more accurate  
107 representation of the diurnal cycle of the low level cloud cover, and (ii) CALIPSO/CALIOP  
108 data (namely the 2B-GEOPROF-LIDAR product, Mace and Zhang, 2014) to infer the cloud  
109 cover vertical profile and cases when low clouds are under a multi-layered cover.

110 These points serve the overall goal of our study to present a description of the diurnal  
111 cycle of the long dry season low-level cloud cover over Gabon and neighboring countries. It

112 should also provide a baseline to further investigate low-level clouds variability in the region  
 113 as well as their realism in global and regional climate models simulations.

114 Section 2 will introduce the new set of in-situ observations and the satellite datasets,  
 115 section 3 will present an extensive comparison between low-level clouds from SYNOP  
 116 observations and from satellite data, and section 4 will discuss and summarize the main  
 117 findings.



118  
 119 Figure 1. Study region, names of main mountain ranges (terrain elevation from Danielson  
 120 and Gesch, 2011) and location of stations used. The station marker size is proportional to the  
 121 total number of available observations in the period 1971–2019. The altitudes are given in  
 122 meters.

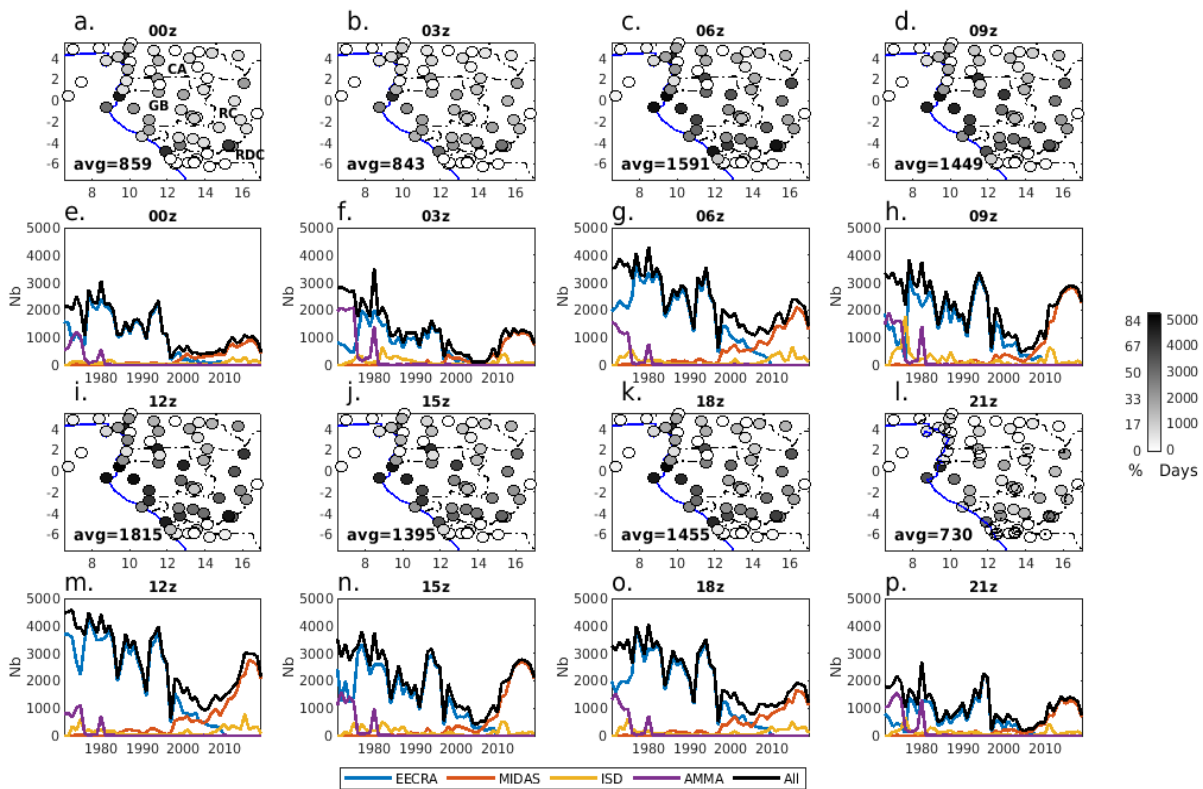
## 123        **2. Data and Methods**

### 124        *a. A comprehensive new dataset of cloud observations from stations*

125        The primary source of observed low-level cloud cover, including the low-level cloud  
126        fraction (LCF) and the low-level cloud genus (LCG), is the “Extended Edited synoptic Cloud  
127        Reports Archive” (EECRA, Hahn et al., 1999; Eastman and Warren, 2014) covering the  
128        period until 2009. LCF is expressed in oktas and is of particular interest for a regional climate  
129        perspective as it governs radiation reaching the surface. LCG uses the World Meteorological  
130        Organization (WMO) coding into nine types (WMO 2019) plus two EECRA-specific types  
131        (11 = obscure sky with fog; 10 = thunderstorm with showers). These two latter types were  
132        omitted in this study (LCF coded to 0) because they result from ancillary information specific  
133        to EECRA and not available in other datasets described below. The WMO low-level cloud  
134        coding comprises cumulus (01 and 02), stratocumulus (04 and 05), stratus (06 and 07),  
135        cumulus and stratocumulus (08), and cumulonimbus (03 and 09). In total, 62 stations were  
136        extracted from EECRA for the period 1971–2009 and the region 5°N–6.5°S/6.5°–16.5°E  
137        (Fig. 1). To fill in gaps and to update the EECRA database to 2019, three other databases  
138        were used; these are in order of priority: The Met Office Integrated Data Archive System  
139        (MIDAS, Met Office 2012), the Integrated surface database (ISD, Smith et al. 2011), and the  
140        African Monsoon Multidisciplinary Analyses information system (AMMA, Fleury et al.  
141        2011). MIDAS is less extensively used than EECRA but a data quality check (not shown) has  
142        revealed better consistency than ISD and AMMA. ISD had some decoding problems from  
143        2013, while our quality control lead us to conclude that AMMA should be given the lowest  
144        priority. EECRA and the three additional sources are based on the same in-situ stations and  
145        are therefore consistent in their common periods of records, as shown with the example of  
146        Libreville (Fig. S1). From the latter three additional sources, three stations not in EECRA  
147        were added: Franceville-Mvengue, Oyem (both in Gabon) and Mbanza Kongo (in Angola).  
148        Inconsistent reports, where either LCG or LCF was zero and the respective other variable was  
149        non-zero, were omitted. We also checked if the cloud observations could be enhanced by  
150        hourly METAR (Meteorological aerodrome Reports) airport reports, but unfortunately the  
151        cloud type coding is different and cloud fraction is not provided in oktas (Fig. S1).  
152        Nevertheless, our merged in-situ cloud observations at synoptic stations (SYNOP  
153        observations) are longer, more complete and more homogeneous than the in-situ observations  
154        used in Dommo et al. (2018). The SYNOP observations have been published alongside this  
155        article (Aellig et al. 2022).



156 SYNOP observations are carried out by trained observers eight times a day at main (00,  
 157 06, 12, and 18 UTC) and intermediate (03, 09, 15, 21 UTC) synoptic hours. Note that the  
 158 local time is UTC+1h. The location of stations, the total number of observations available,  
 159 and their temporal evolution for each source and observation time can be inferred from Fig.  
 160 2. Overall, the number of available observations decreased over time but increased again in  
 161 the late 2000s. Stations in Gabon and Republic of Congo (RC) are the best documented,  
 162 matching with the cloudiest region of WEA (Dommo et al. 2018; Philippon et al. 2019).  
 163 Generally, more daytime (Fig. 2c,d,i,j) than nighttime (Fig. 2a,b,k,l) recordings were  
 164 available (compare 00 UTC to 12 UTC) due to daytime-only operation at several stations.



165  
 166 Figure 2. a-d and i-l: Number of JJAS observations available per stations at 3-hourly time  
 167 steps(maps). The average number of observations for all stations is depicted in the bottom-left  
 168 corner. e-h and m-p: Total number of JJAS observations (all stations) per year and data source  
 169 at 3-hourly time steps (line graphs). Letters in the first panel indicate country names  
 170 (CA=Cameroon, GB=Gabon, RC=Republic of the Congo, RDC= Democratic Republic of the  
 171 Congo).

172 *b. Satellite products*

173 1) CLOUD TYPE FROM SAFNWC

174 The cloud type (CT) product from SAFNWC consists of a classification into 14 types  
 175 available at 3 km spatial and 15-minute temporal resolutions over Europe and Africa from

176 2008 to 2019 (Derrien and Le Gléau, 2005). This product is based on the Spinning Enhanced  
177 Visible and Infrared Imager (SEVIRI), a passive sensor with 12 different spectral channels  
178 on-board the Meteosat Second Generation geostationary satellite (Schmetz et al., 2002). To  
179 construct the SAFNWC CT product, cloud detection and cloud type classification are  
180 performed using series of threshold tests applied sequentially: tests on reflectance and  
181 window channel brightness temperature at 10.8  $\mu\text{m}$  and differences in brightness temperature  
182 between two wavelengths (chosen among 10.8, 12, 3.9, 8.7  $\mu\text{m}$ ). The used thresholds depend  
183 on illumination, viewing geometry and geographical location, and are computed from a  
184 radiative transfer model using ancillary data. Additional tests on spatial and temporal  
185 variability of the brightness temperature at 10.8  $\mu\text{m}$  and spatial variability of the reflectance  
186 are also used. A detailed description of the SAFNWC CT algorithm can be found in Derrien  
187 et al. (2013).

188 In our study, SAFNWC CTs are extracted for the WEA domain 5°N–6.5°S/6.5°–16.5°E  
189 and the 2008–2019 period. For simplification and following Dommo et al 2018, the 14 CTs  
190 were recombined into seven CTs: cloud free, very low clouds (up to 2000 meters above sea  
191 level (a.s.l.)), low clouds (2000–3500 meters a.s.l.), mid-level clouds (3500–6500 meters  
192 a.s.l.), high opaque clouds, high semi-transparent clouds (the latter two higher than 6500  
193 meters a.s.l.), and finally fractional clouds (i.e. small cumulus, thin low or mid-level cloud  
194 edges, very thin high cloud edges, broken and thin mid-level and low-level clouds). Cloud  
195 type maps with the seven types are shown as examples in Figure 3b and 3e for 21 August  
196 2015 12 UTC and 11 July 2010 00 UTC.

## 197 2) NIGHT- AND DAY-MICROPHYSICAL-SCHEMES

198 The Night-Microphysical-Scheme (NMS) and the Day-Microphysical-Scheme (DMS) are  
199 based on radiances and reflectances in the visible and infrared (IR) channels of SEVIRI  
200 (Lensky and Rosenfeld, 2008; Schmetz et al., 2002). The schemes are based on three  
201 different channel combinations, which are combined to RGB composites. The DMS is a  
202 combination of the solar reflectance in the visible channel at 0.8  $\mu\text{m}$  (red) and at 3.9  $\mu\text{m}$   
203 (green), and of the brightness temperature of the IR channel at 10.8  $\mu\text{m}$  (blue). The 0.8  $\mu\text{m}$   
204 channel is a measure of the cloud optical depth and amount of cloud water and ice. The 3.9  
205  $\mu\text{m}$  visible channel is a qualitative measure for cloud particle size and phase (Lensky and  
206 Rosenfeld, 2008). The NMS uses the difference of the brightness temperatures of the IR  
207 channels between 10.8 and 12.0  $\mu\text{m}$  (red), and between 3.9 and 10.8  $\mu\text{m}$  (green), and the  
208 brightness temperature of the IR channel at 10.8  $\mu\text{m}$  represented in blue (Lensky and

209 Rosenfeld, 2008). The channels represented with green are sensitive to particle size of  
210 hydrometeors and the channels represented in red are a measure of the opaqueness of clouds.  
211 Figures 3a and 3d show examples of DMS and NMS for 21 August 2015 12 UTC and 11 July  
212 2010 00 UTC with the RGB NMS and DMS cloud classification by EUMeTrain (2017).  
213 From these schemes, we distinguish for every grid point (3km x 3km) three categories: low  
214 clouds, higher clouds and clear skies. The low-level cloud cover in DMS is determined by a  
215 reflectance of more than 25% in the 0.8  $\mu\text{m}$  visible channel and a brightness temperature  
216 (10.8  $\mu\text{m}$ ) greater than 283 K, while during the night the low-level cloud cover in the NMS is  
217 determined by a difference between the brightness temperature of the channels 12.0 and 10.8  
218  $\mu\text{m}$  greater than 2 K and a brightness temperature of channel 10.8  $\mu\text{m}$  greater than 283 K. The  
219 thresholds for NMS to detect low-level cloud cover have been used already in former studies  
220 (van der Linden et al., 2015). 283 K represents the temperature at about 3000 m a.s.l. in the  
221 study region, likely the upper limit of low-level clouds. In both DMS and NMS, brightness  
222 temperatures lower than 283 K are considered as higher clouds.

### 223 3) CLOUDSAT/CALIPSO CPR/CALIOP (2B-GEOPROF-LIDAR)

224 The 2B-GEOPROF-LIDAR product is a merged product of data from the Cloud-Aerosol  
225 Lidar with Orthogonal Polarization (CALIOP) lidar aboard CALIPSO (Winker et al., 2003)  
226 and the Cloud Profiling Radar (CPR) aboard CloudSat (Stephens et al., 2002). Mace and  
227 Zhang (2014), developed the 2B-GEOPROF-LIDAR product combining both profiles,  
228 getting the most out of the information from both satellites. These two satellites are in the A-  
229 train constellation circling around the earth in about 90 minutes and having a repeat period of  
230 16 days until they sample the same swath again. They scan WEA on an ascending path from  
231 the southeast to the northwest between 12:20 and 13:15 UTC, and on a descending path from  
232 the northeast to the southwest between 23:20 UTC and 00:15 UTC. The time periods  
233 available were JJAS 2006-2017 for daytime and JJAS 2006-2010 for nighttime. The CPR can  
234 penetrate more optically thick clouds, while CALIOP can detect thin clouds and clouds close  
235 to the surface (Mace et al., 2009; Marchand et al., 2008). An illustrative example for West  
236 Africa is given in Knippertz et al. (2011). 2B-GEOPROF-LIDAR has a spatial resolution of  
237 around 1.4 km along track, about 1.8 km cross track, and about 250 m vertically (Mace et al.,  
238 2009). In WEA, the swaths have a zonal distance of around 170 km between each other.

239 4) SPATIAL REPRESENTATION OF THE THREE SATELLITE PRODUCTS

240 To qualitatively illustrate the performance of the different satellite products at day and  
241 night, Fig. 3 provides examples for 1200 UTC 21 August 2015 and 0000 UTC 11 July 2010.  
242 At daytime (top panels), both the SAFNWC and DMS represent the low-level clouds over  
243 Gabon and the adjacent ocean similarly. In the 2B-GEOPROF-LIDAR product, the high  
244 clouds over Cameroon and northern Gabon, likely stemming from deep convection, are  
245 represented by high opaque and semi-transparent clouds in SAFNWC. At night (bottom  
246 panels), the difficulty in the detection of low-level clouds by SAFNWC as opposed to NMS  
247 is clearly visible over central and northern Gabon. 2B-GEOPROF-LIDAR shows the  
248 thickened high-level clouds over the northern part of the region, which potentially prevents  
249 detection of low-level clouds underneath. A close inspection of Fig. 3f reveals that 2B-  
250 GEOPROF-LIDAR can detect low-level clouds underneath higher clouds, if the latter are  
251 thin.

252 5) CLIMATOLOGY OF LOW-LEVEL CLOUD COVER FROM SATELLITES

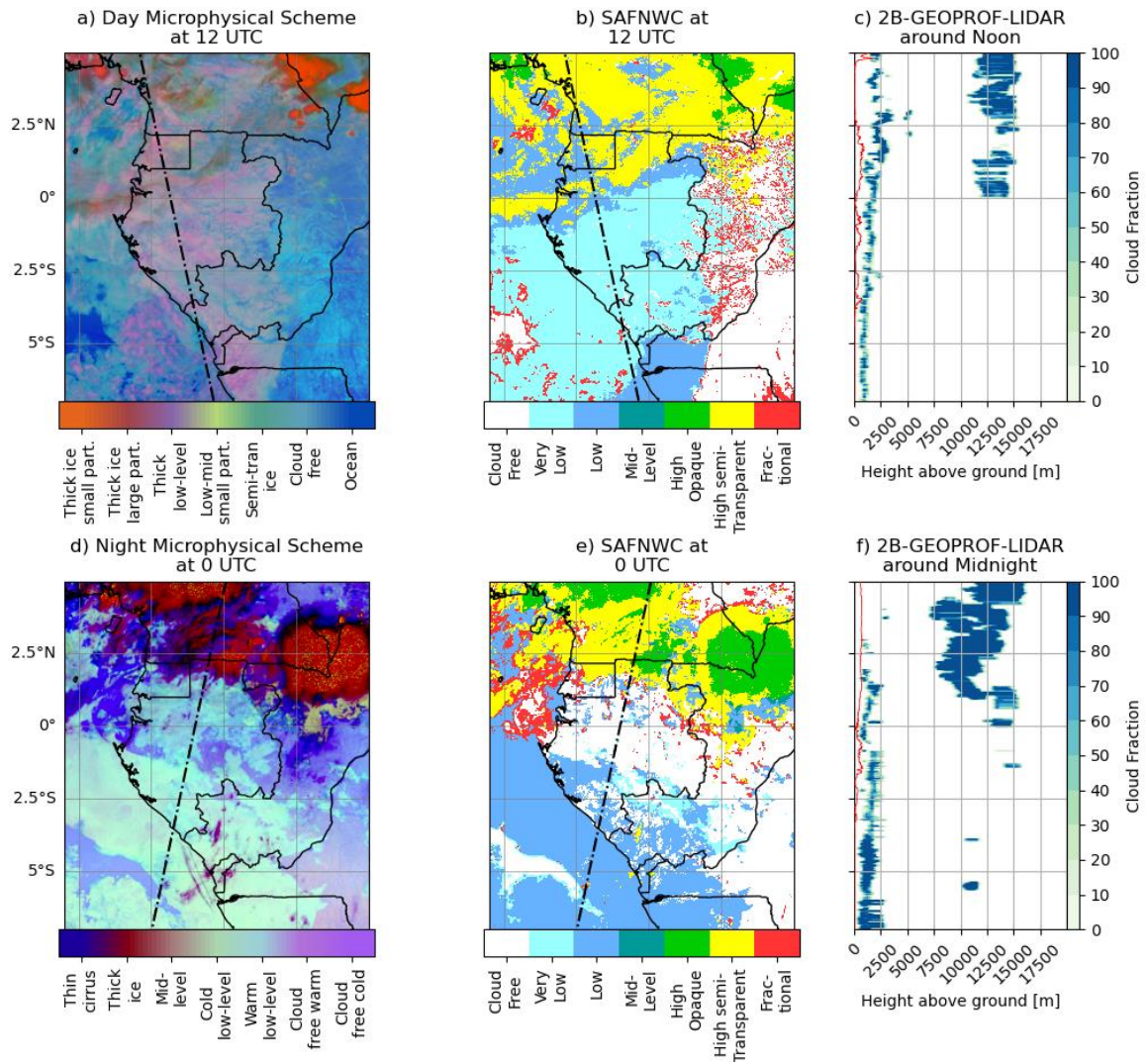
253 The climatology of low-level cloud cover was calculated for SAFNWC, DMS, NMS, and  
254 2B-GEOPROF-LIDAR. These products do not provide LCF data, since only the presence or  
255 absence of clouds in each pixel is detected. Hence, the climatology was primarily based on the  
256 low-level cloud occurrence frequency (LCOF).

257 For SAFNWC, we calculated the average JJAS 3-hourly low-level cloud occurrence  
258 frequency (LCOF) for the types of very low and low-level clouds at each grid point. Very low  
259 clouds (top of the cloud under 2000 meters a.s.l) and low clouds (2000 — 3500 meters a.s.l.)  
260 types are considered together for the calculation of LCOF because the top of the low-level  
261 clouds detected in SYNOP (i.e. stratocumulus) can be situated above 2000 meters a.s.l. This  
262 choice highlights the difficulty of comparing low level clouds from ground observations and  
263 from satellites. At stations, clouds are seen from the ground and therefore determined according  
264 to their base height (low, middle or high level) and type (9 possible categories). Cumulonimbus  
265 clouds are for instance reported by WMO as low clouds (i.e. with a base height below 2000m  
266 a.s.l.) despite their vertical extension. With satellites, clouds are determined according to their  
267 top height, so cumuliform clouds are often classified as higher clouds and low clouds are  
268 masked in case of a multilayered cloud cover. Therefore, the mismatch between ground  
269 observations and satellite estimates of low level clouds can be quite large in the presence of  
270 cumulus, cumulonimbus, or a multilayered cloud cover. The grid points characterized by

271 fractional clouds were also reassigned to another cloud type when at least half of the eight  
272 surrounding points belonged to that type, following the method in Dommo et al. (2018). This  
273 reassignment was made because the number of fractional clouds is not negligible and this type  
274 appears spatially as a transition between two types (cf. Fig. 3). LCOF at each grid point and  
275 observation time was obtained by calculating the ratio of the number of occurrence of very  
276 low-level, low-level or reassigned fractional days to the total number of days, excluding higher  
277 clouds (mid, high opaque and high semi-transparent). This method counters the problem of  
278 low-level clouds not detected due to clouds situated above. The higher-level cloud occurrence  
279 frequency was also calculated from the ratio of occurrence number of mid, high opaque, and  
280 high semi-transparent cloud types to the total number of days.

281 For the climatology of low-level cloud cover based on NMS and DMS, we calculated for  
282 each grid point the average JJAS 3-hourly LCOF with the thresholds defined in section 2.b.2.,  
283 but only using the data with a threshold of the brightness temperature ( $10.8 \mu\text{m}$ ) greater than  
284 283 K. With this approach we alleviated the problem of clouds situated above the low-level  
285 clouds, similarly to the approach used to calculate LCOF from SAFNWC.

286 For the climatology of low-level cloud cover based on 2B-GEOPROF-LIDAR, we  
287 calculated first the cloud fraction and the cloud occurrence frequency at each vertical level  
288 (250m resolution) and for each  $0.5^\circ$  parts (roughly 56 km) along track of the swaths (see  
289 section 2.b.3.) using the random-overlap method (Geleyn and Hollingsworth, 1979; Räisänen  
290 et al., 2004). For the lowest 3000 meters a.s.l., we calculated the climatology of LCF and  
291 LCOF with the maximum-random-overlap method (Geleyn and Hollingsworth, 1979). If  
292 there were multiple contiguous low-level clouds present, the random overlap method  
293 (Räisänen et al., 2004) was applied. These overlap assumptions follow the method used in  
294 van der Linden et al. (2015).



295

296 Figure 3. Satellite products on 1200 UTC 21 August 2015 (a-c), and 0000 UTC 11 July  
 297 2010 (d-f) representing Cloud types from Day-Microphysical-Scheme (a), Night-  
 298 Microphysical-Scheme (d), and SAFNWC (b and e); and cloud height and fraction from 2B-  
 299 GEOPROF-LIDAR (c and f). The black dotted line in a-b and d-e depicts the path of the  
 300 satellite, the data of which are shown in panels c and f. The red line in c. and f. represents the  
 301 elevation.

### 302 *c. Methods for comparing in-situ observations and satellite products*

303 Low-level cloud fraction (LCF) and low-level cloud genus (LCG) at synoptic weather  
 304 stations (SYNOP observations) are assessed by trained observers. Despite the subjective  
 305 assessment and problems at night due to low illumination, various previous studies have  
 306 shown their great value in obtaining cloud climatology and verification against satellite  
 307 observations over Africa (van der Linden et al. 2015).

308 For the comparison with satellite products, the LCF climatology was calculated at synoptic  
 309 weather station for time steps when the cloud genus (LCG) was either “stratocumulus” (genus

310 4-5), “stratus” (6–7), or “stratocumulus and cumulus” (8). For all other low-level cloud genus  
311 (1, 2, 3, 9, i.e. cumulus and cumulonimbus clouds), the corresponding low-level cloud fraction  
312 was set to 0 oktas because these clouds are not strictly low-level clouds and likely seen as  
313 higher clouds from the satellites. Note that genus 1 (cumulus humilis), is rare, as its frequency  
314 of occurrence is less than 2% at night and about 6% at daytime. Thus, using cloud genera 4–8  
315 for stratiform low-level clouds at stations and comparing it with satellite low-level clouds  
316 appears a tolerable inconsistency. The Low cloud occurrence frequency (LCOF) for SYNOP  
317 observations was calculated by counting the occurrence of LCF higher than 4 oktas. For the  
318 evaluation of satellite products against SYNOP observations, we converted cloud occurrence  
319 around SYNOP stations to cloud fraction. We took the distance-weighted (cosine function from  
320 0 to  $\pi/2$ ) average cloud fraction in a radius of 20 km around the station at the time of the  
321 observation, under the assumption that the observer on the ground can classify clouds and their  
322 fractional cover in the sky up to this distance (WMO, 2019). Very low clouds, low clouds and  
323 fractional reassigned clouds (see section 2.2.5) are considered together for the calculation of  
324 low cloud fraction, similarly to the calculation of LCOF described in section 2.2.5. For the  
325 comparison of low-level cloud fraction from SYNOP observations and satellite data, days with  
326 more than 50% of higher clouds in the 20km radius around a station were excluded from the  
327 analysis. This condition was applied because high- and mid-level clouds prevent the detection  
328 of lower clouds from the satellites.

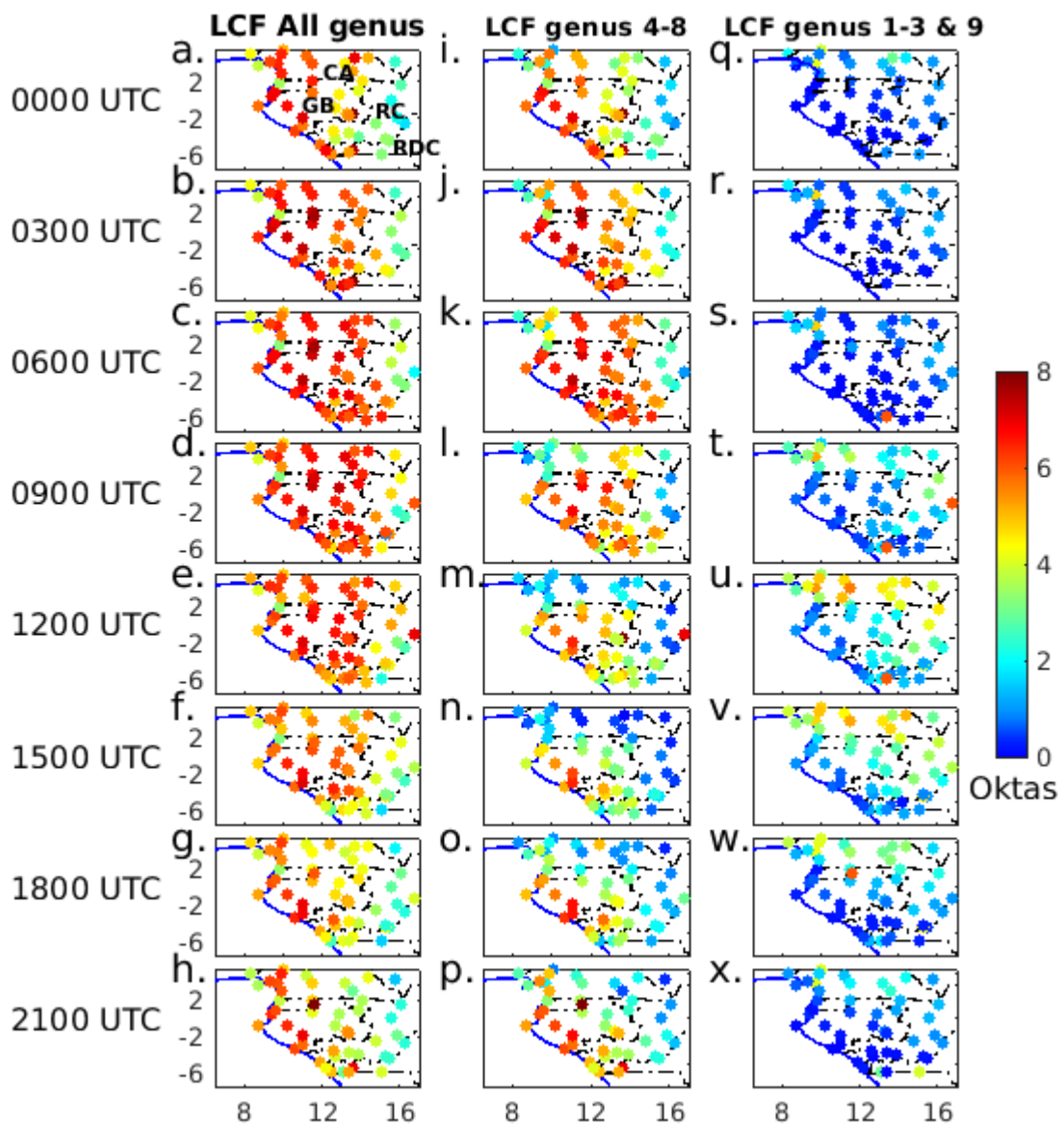
### 329 **3. Results**

330 This section shows in four parts the diurnal cycle of low-level clouds in WEA. The  
331 first two parts explore the low-level cloud fraction and low-level cloud genus from SYNOP  
332 observations on one hand and then the low-level cloud occurrence frequency from the three  
333 satellite datasets on the other hand. The third part shows a comparison between SYNOP  
334 observations and satellite data. The last part thoroughly compares the day and night evolution  
335 of low-level clouds from SYNOP observations and satellite data.

#### 336 *a. Ground observations of low-level cloud fraction and genus*

337 The long-term (JJAS 1971–2019) mean diurnal cycle of low-level clouds fraction (LCF) is  
338 provided in Fig. 4. LCF with non-cumuliform clouds only (i.e. low topped low clouds, genus  
339 4-8, Fig.4 i-p) and with only cumuliform clouds (genus 1-3 and 9, Fig. 4q-x) are also shown.  
340 Taking LCF calculated from all genus, the cloud fraction is clearly lower toward the Congo

341 Basin in the east (Fig. 4a-h). In eastern Gabon, eastern Cameroon and southwestern RC, LCF  
 342 increases at night (Fig. 4h,a,b), remains high until noon (Fig. 4e), and is followed by a decrease  
 343 in the afternoon (Fig. 4f-g). When taking non cumuliform clouds only (Fig. 4l-n) the decrease  
 344 is more pronounced and occurs earlier in eastern Gabon and Cameroon, showing that these  
 345 regions are affected by convection and the development of cumuliform clouds in the daytime  
 346 (Fig. 4t-v).

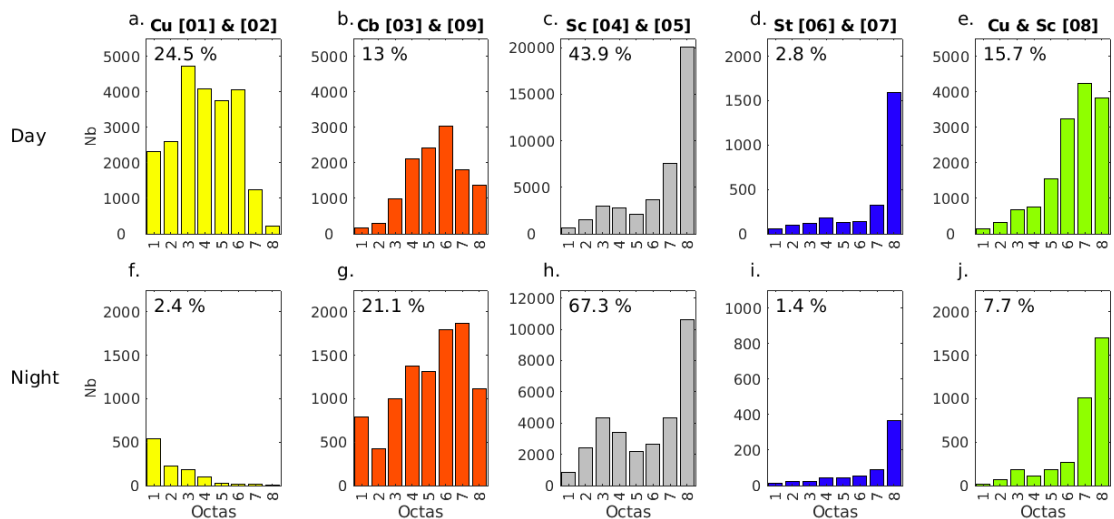


347  
 348 Figure 4. JJAS (1971–2019) SYNOP low-level cloud fraction calculated from all genus (a-  
 349 h), genus 4–8 only (i-p) and genus 1-3,9 only (q-x) per station and observation time.

350 The occurrence of cloud genus from SYNOP observations furnishes additional  
 351 information regarding the type of low-level cloud cover in WEA (Fig. 5). Stratocumulus (Sc,



352 genus 04 and 05) is by far the most frequent type at night time (UTC 1800 – UTC 0300)  
 353 representing two thirds of all cloud genus (Fig. 5f-j). The second most frequent cloud genus  
 354 at night is cumulonimbus (Cb, genus 03 and 09) occurring at 21.1% of all observations.  
 355 During daylight (UTC 0600 – UTC 1500, Fig. 5a-e), stratocumulus is less prominent but  
 356 remains the most frequent (44%) followed by “cumulus humilis” and “mediocris” (Cu, genus  
 357 01 and 02, 24.5%). The other main type is “cumulus and stratocumulus” (Cu & Sc, genus 08,  
 358 15.7%). The occurrence of stratus (St, genus 06 and 07) is very low (1 to 3%) during day and  
 359 night (Fig. 5d,i). It is likely that many clouds referred to as stratocumulus by observers are  
 360 stratus. In any case stratus and stratocumulus are both counted as stratiform low level clouds.  
 361 These results show that a significant number of low-level clouds are convective (Cu and Cb  
 362 represent together 37.5% of all genus during the day and 23.5% at night). However, the  
 363 portion of the sky covered by Cu and Cb is generally lower than Sc (oktas, x-axis of Fig. 5).  
 364 Stratocumulus and stratus show a frequency distribution skewed to higher sky coverage (7-8  
 365 oktas, Fig. 5c-d and Fig. 5h-i). For cumulus, the distribution shows a higher frequency  
 366 between 3 and 6 oktas and a distribution even skewed to lower cloud coverage (Fig 5a). The  
 367 distribution of Cumulonimbus is centered around 4-7 oktas but is skewed to higher cloud  
 368 coverage during the day (Fig. 5b) while the distribution is flatter at night (Fig. 5g).

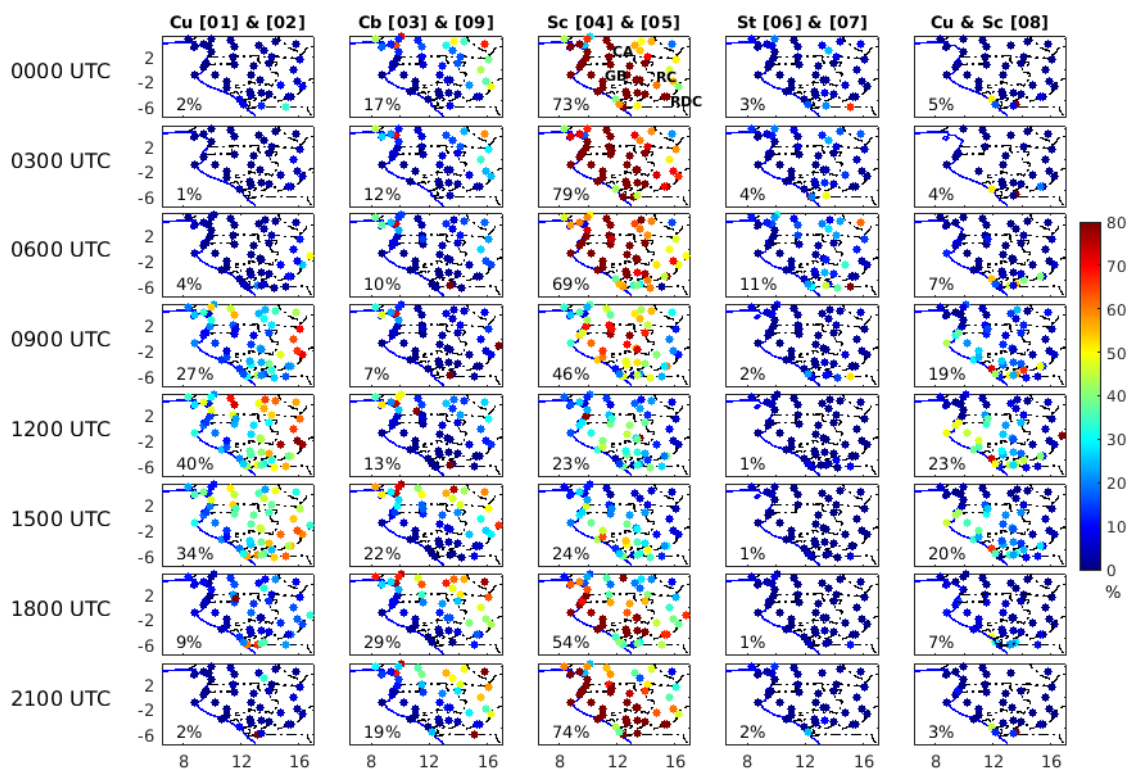


369

370 Figure 5. JJAS (1971-2019) number of SYNOP observations low-level cloud genus by  
 371 oktas from all stations for daytime (06–15 UTC, a-e) and night-time (18–03 UTC, f-j).  
 372 Percentages at the top give the frequency for each type over all SYNOP observation times.

373 The frequency of the cloud types varies spatially throughout the day (Fig. 6). At night (1800  
 374 – 0300 UTC), the frequency of stratocumulus (genus 4 and 5) is high (>70%) especially in  
 375 western Cameroon, Gabon and southwest RC. Some exceptions such as Porte-Gentil, show a

376 lower amount of Stratocumulus at night. The simultaneous higher amount of Sc and Cu (genus  
 377 8), suggest that a specific cloud referencing by the observer in Port-Gentil might be the cause  
 378 of this difference. In the morning, the amount of Sc markedly decreases everywhere but stays  
 379 relatively high in the central part of Gabon. Simultaneously, the amount of cumulus (genus 1  
 380 and 2) increases, especially in Cameroon and RC, where it reaches a maximum around 1200  
 381 UTC. The cumulus & stratocumulus genus (genus 8) also reaches a maximum around 1200  
 382 UTC, but occurs more frequently near the coast of Gabon. It reflects the breaking of the  
 383 stratocumulus deck in the course of the day. Further, the stratus deck is more persistent on the  
 384 windward slope of the Chaillu massif. The frequency of cumulonimbus (genus 3 and 9)  
 385 increases later, reaching a maximum around 1800 UTC, located mostly in Cameroon and RC,  
 386 while staying very low near the coast of Gabon and RC.



387

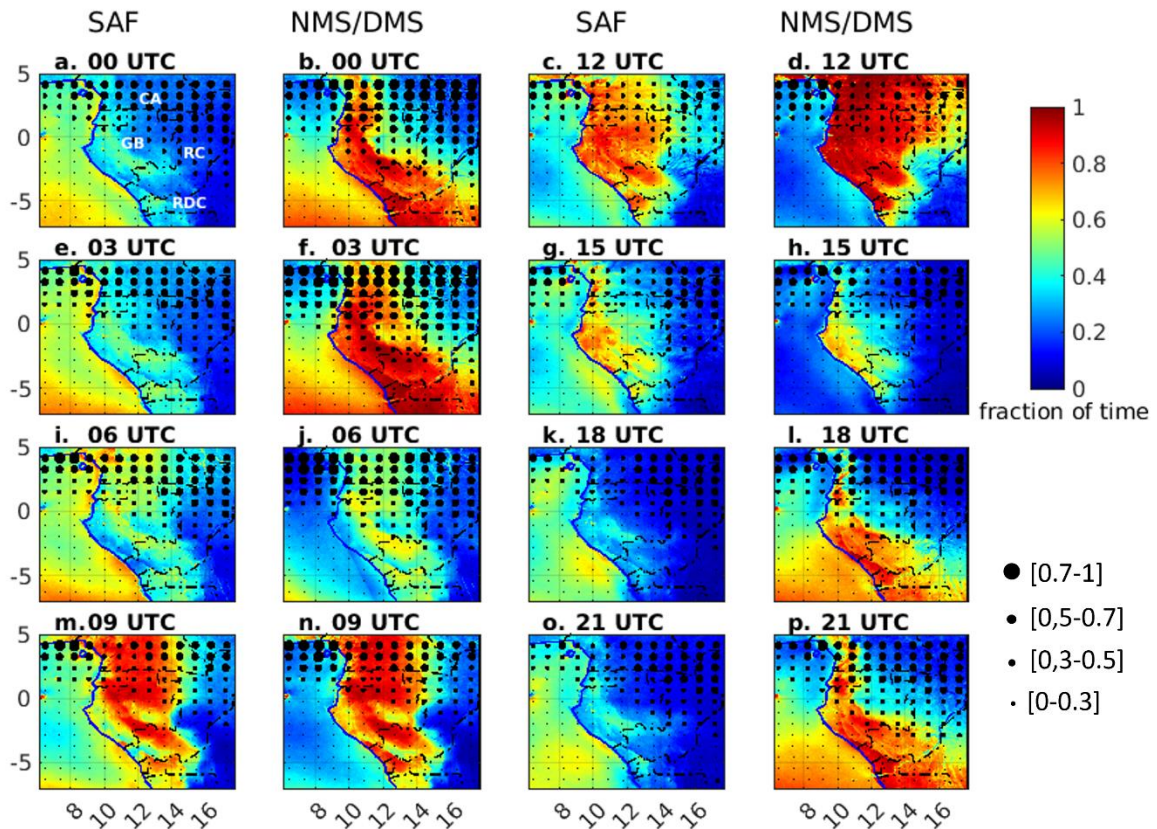
388 Figure 6. JJAS (1971–2019) SYNOP cloud genus occurrence frequency per station and  
 389 observation time. For each panel, the number at the left bottom shows at each observation time  
 390 the average fraction of the given cloud genus.

391 *b. Satellite observations of horizontal and vertical distributions of low-level clouds*

392 The average diurnal evolution of low-level cloud occurrence frequency (LCOF) from  
 393 SAFNWC and NMS/DMS are displayed in Fig. 7 at the same 3-hourly time steps as in figure  
 394 4. Between 0600 UTC and 0900 UTC, LCOF increases dramatically in both products (Fig.  
 395 7i-j and 7m-n), likely associated with the low solar angle that prevents the satellite from

396 satisfactorily detecting low-level clouds just after the sunrise. This effect is conspicuous in  
397 the first hour of daylight with a large LCOF increase observed between 0600 UTC and 0700  
398 UTC (Fig. S2). In DMS, the increase of LCOF continues between 0900 UTC and 1200 UTC,  
399 especially in Cameroon (Fig. 7n,d). Between 1200 UTC and 1500 UTC LCOF decreases in  
400 the entire area, quite sharply with DMS (Fig. 7d,h), but stays high in western Gabon mainly  
401 in SAFNWC (Fig. 7c,g). The lower LCOF in the eastern part of the region in the afternoon  
402 suggests a sky clearing likely due to a transition from stratocumulus to cumulus shown in  
403 SYNOP (Fig.6). Between 1500 UTC and 1800 UTC, corresponding to the period of the  
404 switch from the DMS to the NMS, the evolution of LCOF is different between the two  
405 satellite products SAFNWC (Fig. 7g,k) and the DMS/NMS microphysical scheme (Fig. 7h,l).  
406 While the LCOF continues to decrease during sunset in SAFNWC (a constant decrease  
407 according to Fig. S3), the LCOF starts to increase again in DMS/NMS, mainly in the coastal  
408 area. After 1800 UTC and throughout the night LCOF increases again in both products, but  
409 LCOF levels in NMS (Fig. 7b,f,l,p) are almost twice those of SAFNWC (Fig. 7a,e,k,o). The  
410 increase of LCOF in NMS is again remarkable over the windward slopes and summit of the  
411 main mountain ranges and the coast of RC and RDC and has a wider expansion along the  
412 Chaillu Massif between 0000 UTC and 0300 UTC (Fig. 7b,f).

413 The higher-level cloud occurrence frequency (HCOF) from SAFNWC and NMS/DMS is  
414 also shown in Fig.7 (black dots) and points out the areas of higher uncertainty in the detection  
415 of low-level clouds from satellites. HCOF is larger in Cameroon, northern RC and northern  
416 Gabon in both products and is increasing at night, reaching a 70% occurrence frequency in  
417 Cameroon under NMS.

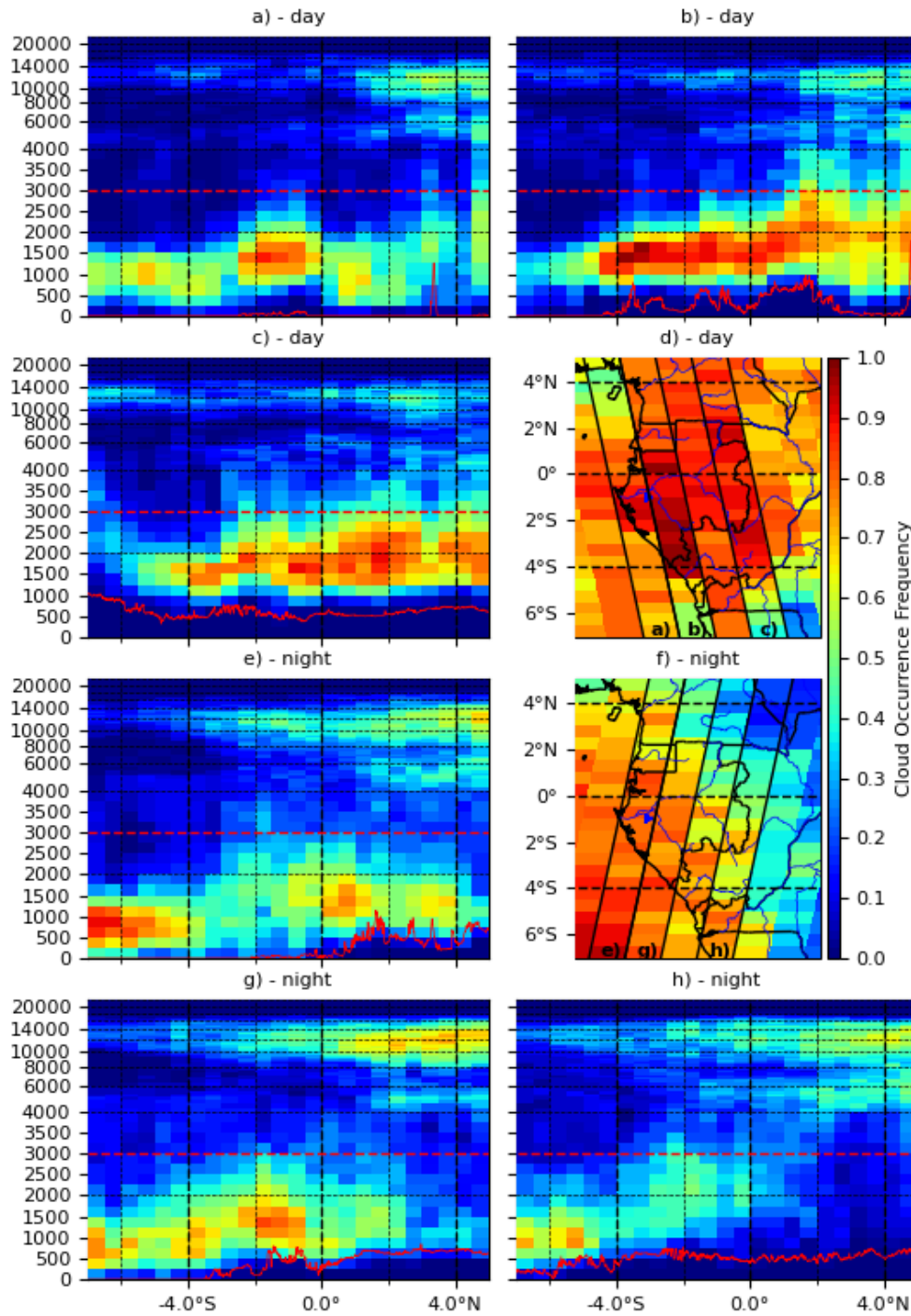


418  
 419 Figure 7. JJAS Low-level clouds occurrence frequency (shading) and high clouds (dots)  
 420 from SAFNWC and NMS/DMS for the eight observation times available at the analyzed  
 421 stations in the period 2008–2019.

422 The twice-daily 2B-GEOPROF-LIDAR product does not allow to investigate the full  
 423 diurnal cycle of the low-level cloud cover. However, it brings valuable information about  
 424 clouds height, thickness and multilayers. Therefore, Figure 8 displays climatologies for  
 425 around 12,30 UTC and 00,30 UTC of the vertical distribution (till 20km) of cloud occurrence  
 426 frequency for six paths, and maps of LCOF (0-3000 meters a.s.l.). Around noon, the spatial  
 427 variability of LCOF (Fig. 8d) is similar to the LCF (Fig. S4) and also similar to SAFNWC  
 428 and DMS (Fig. 7c. and 7g.), namely a widespread stratiform deck in Gabon, the western part  
 429 of RC and southwestern Cameroon. The main difference compared to SAFNWC is a larger  
 430 number of low-level clouds near the coast of Gabon in 2B-GEOPROF-LIDAR (Fig. 8d). The  
 431 vertical distribution of clouds also shows more low-level clouds from the coastal plains to the  
 432 west of the Chaillu Massif (Fig. 8b, 4°S-2°N). The other main feature is a higher base of low-  
 433 level clouds over land (Fig. 8b-c) compared to the ocean (Fig. 8a), which might be due to the  
 434 elevated terrain (red line curves in Fig. 8a-c). The low-level clouds are also thicker north of  
 435 2°S (up to 3000 meters). In addition, multilayered higher clouds become more frequent  
 436 towards northern areas (Fig. 8a-c) and mask the low-level clouds when detected by passive  
 437 sensors onboard satellites.

438 At mid-night the LCOF from 2B-GEOPROF-LIDAR (Fig. 8f) shows generally less low-  
439 level clouds than at noon (Fig. 8d). A close inspection of Fig. 4i and 4m over central Gabon  
440 corroborates this finding, only later in the night and in the early morning the LCOF increases  
441 further and peaks in the diurnal cycle. In addition, the low-level clouds are more frequent near  
442 the coast and their amount decreases inland towards the east (Fig. 8f), which is consistent with  
443 the results found with SAFNWC (Fig. 7a,e,o) and NMS (Fig. 7b,f,p). The clouds might be  
444 advected inland from the ocean, but because of the scarce twice-daily over-flights the dynamics  
445 of the low-level clouds are difficult to estimate by 2B-GEOPROF-LIDAR. The vertical  
446 distribution of clouds confirms the expanded stratus deck to the west, i.e. on the windward  
447 slopes (Fig. 8e,g) while over the plateau further east (Fig. 1), the low-level cloud fraction is  
448 lower (Fig. 8h). The role of the topography is shown here clearer compared to daytime (Fig.  
449 8a-c), likely due to the SW-NE orientation of 2B-GEOPROF-LIDAR path followed at night  
450 (Fig. 8f). In all night paths, there are also larger amounts of high level clouds over northern  
451 Gabon, northern RC, and Cameroon (Fig. 8e,g-h), consistently with SAFNWC and NMS (Fig.  
452 7a-b).

453 The results suggest a widespread stratiform cloud deck in the morning that clears up in  
454 the afternoon mainly in the plateau east of Chaillu massif and Cristal mountains. However,  
455 some inconsistencies between products have been found mainly due to the inability of  
456 SAFNWC to detect low-level clouds at night. The multi-layered cloud cover mostly present  
457 in northern Gabon and southern Cameroon at night as seen from 2B-GEOPROF-LIDAR,  
458 may partly explain the lower number of low-level clouds detected with SAFNWC and  
459 NMS/DMS there compared to SYNOP observations (Section 3.1). The aim of the next  
460 section is to thoroughly compare SYNOP observations and satellite data.



461

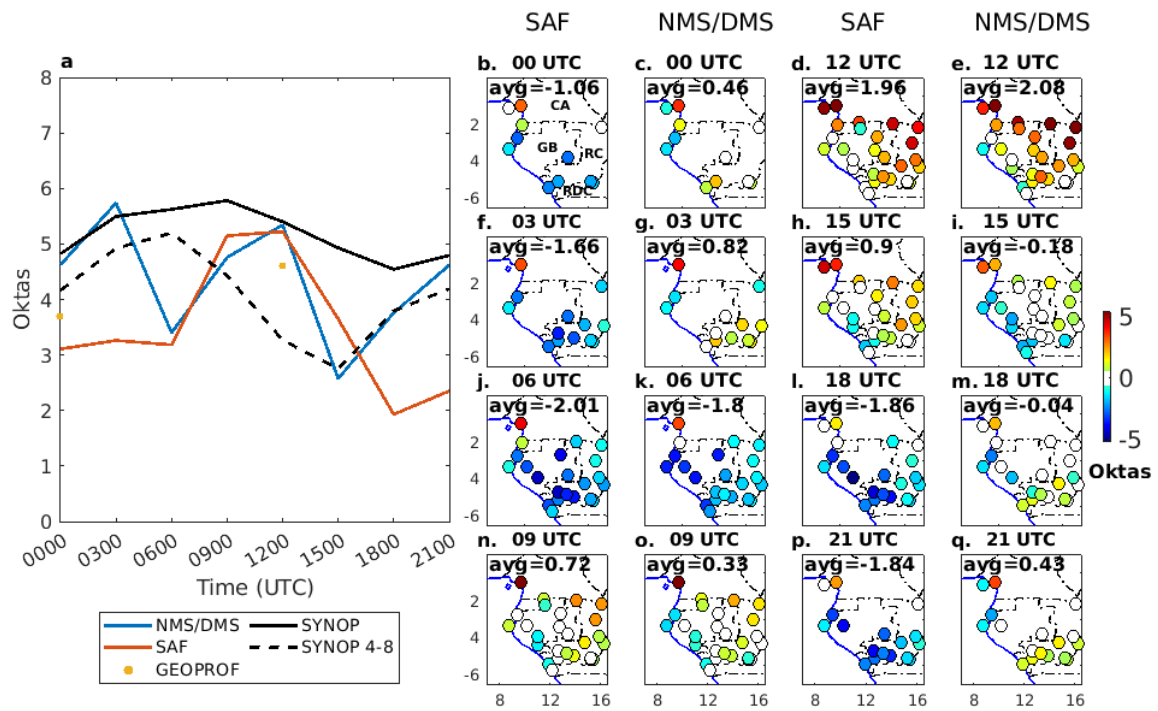
462 Figure 8. JJAS vertical cloud occurrence frequency from 2B-GEOPROF-LIDAR along  
 463 three paths at 12:30 UTC (a,b,c) and three paths at 00:30 UTC (e,g,h) for the period 2006-2017  
 464 during the day and 2006-2010 during the night. The red line is the topography. The LCOF  
 465 calculated in each swath between the ground level and 3000 meters a.s.l. (horizontal red dotted  
 466 line) are shown at 12:30 UTC (d.) and 00:30 UTC (f.)

467 *c. Comparison of satellite and station observations*

468 In this section, LCF from satellites and from SYNOP observations are compared. The  
 469 average LCF in the entire area is very different between a LCF calculated with all SYNOP

470 genus or excluding cumuliform clouds (genus 4 to 8 only). During the day (1200 UTC-1500  
471 UTC) the LCF excluding cumuliform clouds is lower by approximately 2 oktas. Focusing on  
472 the latter, the highest level (more than 5 oktas) is reached at 0600 UTC (Fig. 9a). The LCF  
473 decreases during the day to reach a minimum at 1500UTC (3 oktas). The diurnal cycle of LCF  
474 from satellites is similar between SAFNWC and DMS during the day (0600 UTC – 1500 UTC,  
475 Fig. 9a) with a peak at midday. In the early morning (0600 UTC) when the solar angle is low,  
476 both satellite products underestimate the SYNOP observations because of a low illumination.  
477 LCF from satellites overestimates SYNOP observations at midday (1200 UTC) when  
478 cumuliform clouds are not counted in SYNOP observations (Fig. 9a). In the afternoon, satellite  
479 products show a decrease of LCF, reaching a number close to SYNOP observations (around 3  
480 oktas at 1500 UTC). At night (1800 UTC to 0300 UTC), LCF from SAFNWC shows a large  
481 underestimation (2 oktas) compared to SYNOP observations while NMS show closer results  
482 to SYNOP observations (Fig. 9a).

483 The bias between satellite datasets and SYNOP observations is highly dependent on the  
484 region (Fig. 9b-q). At 0600 UTC the underestimation of LCF from satellites is larger in  
485 western RC and western Gabon (Fig. 9j,k). During the day LCF starts to be overestimated  
486 mainly in the north-east part of RC (Fig. 9n,o,d,e,h,i), where the cumuliform clouds are more  
487 prevalent (Fig.6). At night (1800 UTC – 0300 UTC) less stations have a sufficient amount of  
488 data for the analysis (mainly in central Gabon), which degrades the accuracy of the results,  
489 but regional variability is still appearing. In western RC, a large underestimation appears in  
490 SAFNWC (Fig. 9l,p,b,f) while NMS shows a slight overestimation (Fig. 9m,q,c,g). On  
491 coastal Gabon, LCF is underestimated by a similar amplitude in both products. The bias in  
492 termu of LCOF was also calculated (Figure S5) and show similar results. In addition, a  
493 statistical analysis of the comparisons between SYNOP observations and satellite data is  
494 shown in Fig. S6.



495

496 Figure 9. a. Spatially averaged diurnal cycle of LCF from SAFNWC, NMS (1800 UTC –  
 497 0300 UTC), DMS (0600 UTC – 1500 UTC) and SYNOP observations (all genus and genus 4  
 498 to 8 only). All stations have the same weight regardless of their sample size. b-q. Maps of the  
 499 mean bias (in oktas) between LCF from SAFNWC or NMS/DMS and SYNOP observations  
 500 (genus 4 to 8) for the period JJAS 2008–2019. “Avg” represents the average bias from all  
 501 stations. The stations with less than 10% of available data have been removed from the analysis  
 502 for each observation time.

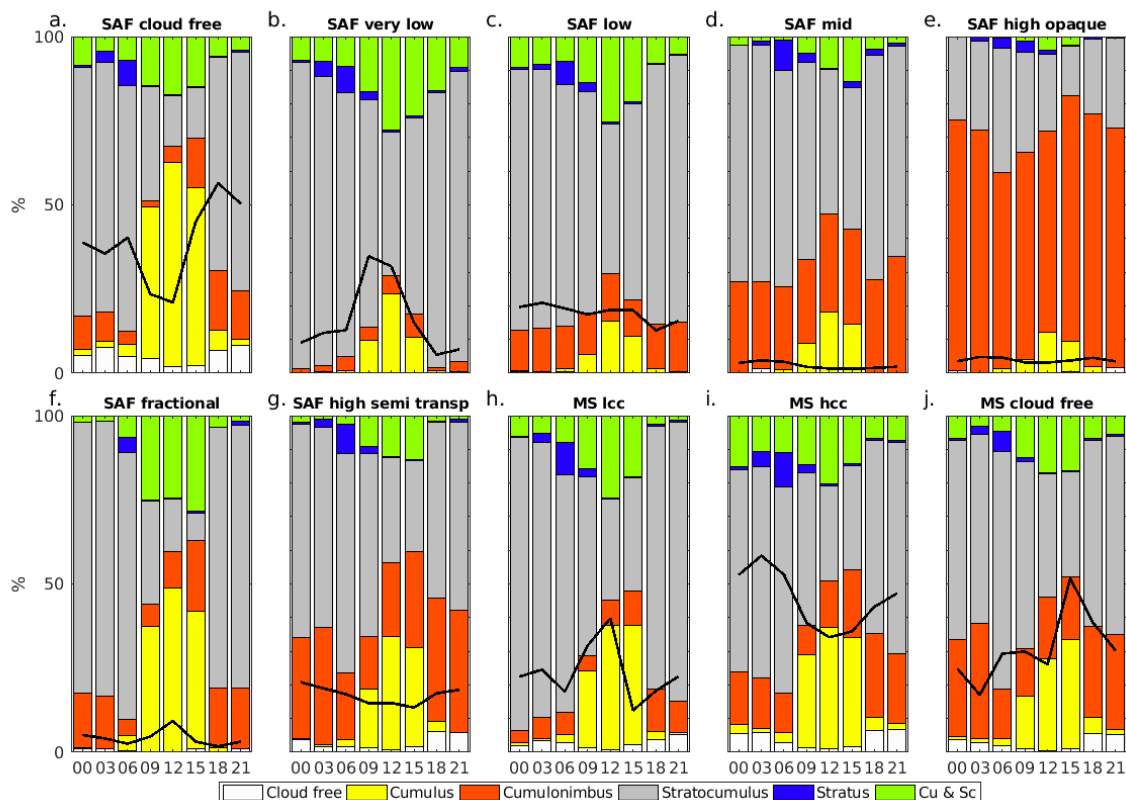
503 The occurrence of low cloud genus from SYNOP observations and the occurrence of low  
 504 cloud types from satellite data are finally compared to investigate how the satellites detect the  
 505 different cloud genus. Figure 10 displays the diurnal cycle of the frequency of low-level  
 506 cloud genus as observed at the stations (colored bars) for each satellite cloud type (individual  
 507 panels).

508 Very low and low clouds together are the most frequent SAFNWC cloud types during the  
 509 day (black line, Fig. 10) and are mostly detected when non-convective clouds  
 510 (Stratocumulus) are observed from the ground (gray shade, Fig. 10b-c). Cloud free is detected  
 511 more frequently at night and early morning (1800 UTC to 0600 UTC) and corresponds also  
 512 mostly to stratocumulus (Fig. 10a), showing that a large part of stratiform clouds observed  
 513 from the ground are not well detected by SAFNWC at night. As previously discussed in van  
 514 der Linden et al. (2015), this is partly related to small temperature differences between low-  
 515 level clouds and the ground, making it difficult to detect low-level clouds using IR brightness  
 516 temperatures. In addition, high water vapor content in low levels makes it difficult to adjust



517 thresholds to detect cloudy pixels. During the day (0900 to 1500 UTC), Cumulus clouds  
 518 prevail when no cloud is detected in satellites (Fig 10a.). Cumulus clouds are also frequent in  
 519 the fractional type (Fig. 10f) due to the fractional characteristic of cumulus. Cumulus covers  
 520 only a part of the sky (Fig. 5), so they are likely to be classified as cloud free in SAFNWC  
 521 (Fig. 10a). The type “high semi-transparent” is also well represented and occurs steadily  
 522 during the day at a frequency between 15 and 20% (black line, Fig. 10g). These high clouds  
 523 from SAFNWC are associated with a significant number of stratocumulus in SYNOP  
 524 observations (Fig. 10g) showing that the high clouds are likely hiding part of the  
 525 stratocumulus situated underneath and seen from the ground.

526 The three DMS/NMS types include low-level clouds (MS lcc), higher level clouds (MS  
 527 hcc) and cloud free (MS cloud free). These types have more inter-types similarities than  
 528 SAFNWC in terms of partition of SYNOP cloud genus. The main difference among  
 529 DMS/NMS types is a slightly higher proportion of stratocumulus in the low-level cloud type  
 530 and a higher proportion of cumulonimbus in the cloud free type (Fig. 10h–j).



531

532 Figure 10. All stations diurnal partition of the SYNOP low-level cloud genus (colored  
 533 bars) in the seven SAFNWC (“SAF” panels) and the three NMS/DMS (“MS” panels) cloud  
 534 types for the period JJAS 2008–2019. The NMS was used from 18–03 UTC and the DMS  
 535 from 06–15 UTC. Black line is the frequency of each SAFNWC cloud type relative to the

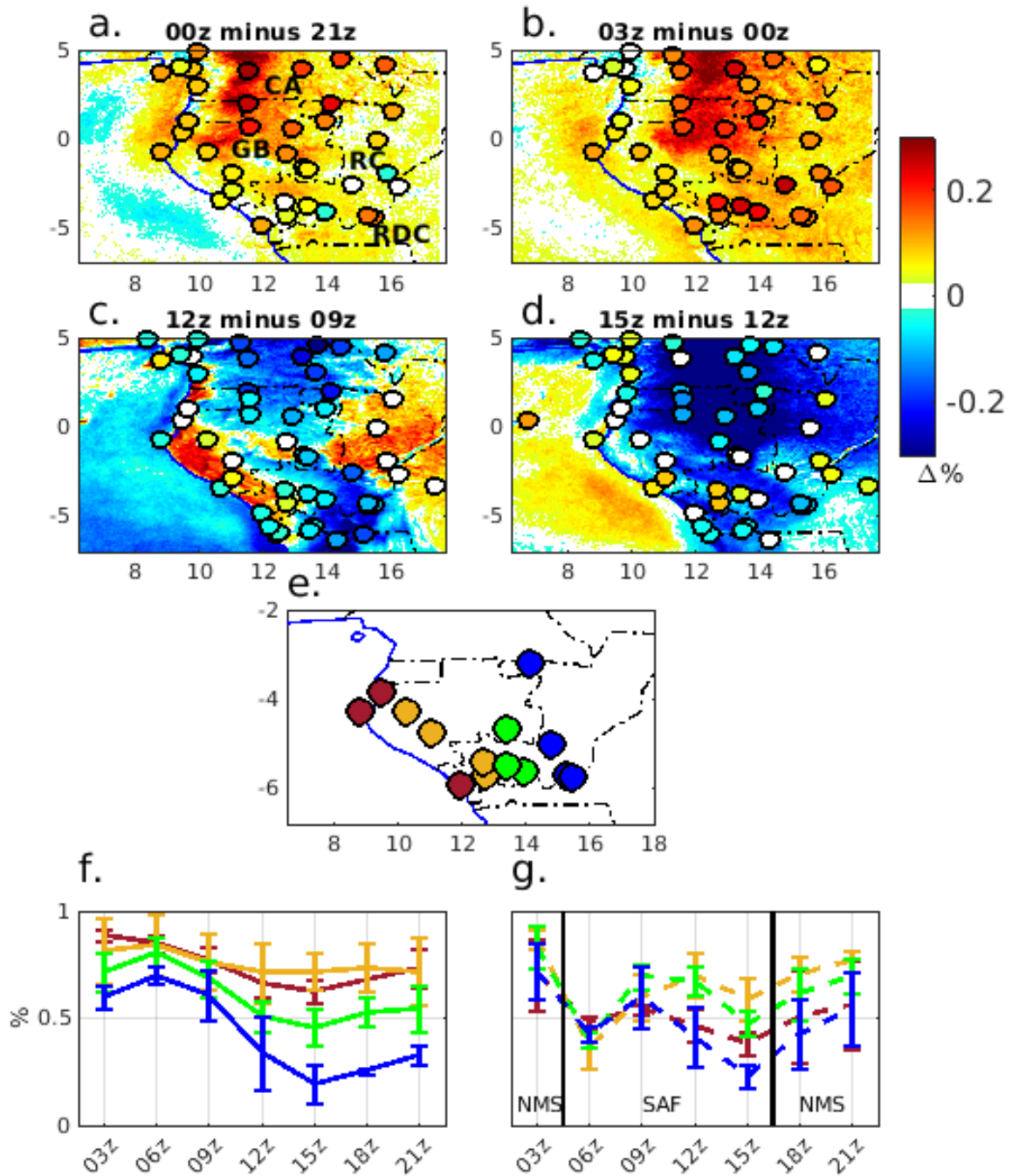
536 number of all available SYNOP observation days and stations. The stations with less than  
537 10% of available data have been removed from the analysis for each observation time.  
538

539 Overall, the comparison between SYNOP observations and satellite data described in this  
540 section suggests clearly that NMS is more realistic than SAFNWC in detecting the low-level  
541 clouds at nighttime. During the day, SAFNWC show similar LCF bias than DMS (Fig. 9) but  
542 shows a higher proportion of stratocumulus detected as low clouds (Fig. 10).

#### 543 *d. Spatial variability in the diurnal cycle of low-level cloud cover*

544 The previous section has shown large differences between SYNOP observations and  
545 satellite products in absolute values of low-level cloud cover. Quantifying the change of low  
546 cloud cover between successive observation times may therefore better reveal the spatial  
547 consistencies of diurnal cycles in the different products. In this section, the evolution of JJAS  
548 low-level cloud occurrence frequency (LCOF) between successive observation times in the  
549 period 2008-2019 using NMS, SAFNWC and SYNOP observations is investigated (Fig. 11).  
550 NMS is used for night time (Fig. 11a,b) and SAFNWC for day time (Fig. 11c,d) because these  
551 products are more reliable in these respective periods, as shown in the previous section. 1800  
552 UTC and 0600 UTC have been removed from this analysis since these times are not well  
553 captured by the satellites (Fig. 9), due to twilight conditions.

554 The results from SYNOP observations show that low cloud occurrence frequency  
555 increases in the evening, starting from western Gabon and western Cameroon, and spreading  
556 to the east (Fig. 11a,b). The results from the NMS satellite data show a similar spatial  
557 variability before midnight with the largest LCOF increase in the Cristal Mountains in  
558 northern Gabon and in south-central Cameroon (Fig. 11a). After midnight and until 0300  
559 UTC, the cloudiness keeps increasing in these regions, but also increases further east (Fig.  
560 11b).



561

562 Figure 11: Change of low-level cloud occurrence frequency (LCOF) compared to the  
 563 previous observation time for NMS (a-b) at nighttime and SAFNWC at daytime (c,d) for the  
 564 period JJAS 2008-2019. The circles are the in-situ observed change LCOF in the period JJAS  
 565 1971-2019 for stations with less than 10% of missing data. e) Location of the stations  
 566 investigated in f) and g). f)-g): Average and standard deviation of LCOF from SYNOP  
 567 observations (f) and satellites (g) at the coast (red), on the windward slopes and coastal plains  
 568 (orange), on the plateau (green), and leeward slopes of Congo Basin (blue). The vertical lines  
 569 in g) delineate the LCOF calculated from SAFNWC (06-15 UTC) and from NMS (18-03 UTC).

570

571

During the day, the SYNOP observations show generally a decrease of low-level cloud cover, but some stations show a very small change in LCOF, mainly in the central and northern

572 part of RC (Fig. 11c-d), most likely due to the development of low-level cumulus clouds (Fig.  
573 6). A stable LCOF is also evident in the coastal hinterlands on the windward side of the Cristal  
574 and Chaillu mountain ranges (Fig. 11c-d). The spatial variability of low cloud cover diurnal  
575 evolution from SAFNWC is moderately consistent with the SYNOP observations: it shows an  
576 increase in LCOF in the morning (0900 UTC - 1200 UTC) in the central and northern part of  
577 RC and the coastal hinterlands, in regions of very low change of LCOF according to SYNOP  
578 observations (Fig. 11c). Between 1200 UTC and 1500 UTC results from SAFNWC show a  
579 general decrease of LCOF except for the coastal hinterlands, in line with a stable or slight  
580 increase of LCOF in SYNOP observations (Fig. 11d).

581 To investigate the difference of mean diurnal cycle between different regions of the area,  
582 stations with at least 10% of available data for each observation between 0300 and 2100 UTC  
583 have been identified (Fig. 11e) and grouped according to their geographical locations. The  
584 average SYNOP observations and SAFNWC LCOF diurnal cycle for these stations have been  
585 calculated and reported on Fig. 11f and 11g. Looking at the SYNOP data, the coastal stations,  
586 including Pointe-Noire, Mayumba, Port-Gentil and Libreville (in red) show very high LCOF  
587 at night (80%), slightly decreasing during the day reaching 60% at 1500 UTC (Fig. 11f). The  
588 windward slopes of the Chaillu mountains represented by the stations Dolisie, Makabana,  
589 Tchibanga, Mouila and Lambarene (orange, cf. Fig. 1) are the cloudiest and show a steady  
590 LCOF around 70-80%. Stations in the plateau region, including Mouyondzi, Sibiti, Franceville,  
591 Lastoursville, Makokou and Mitzic (green) show a LCOF peaking at 80% around 0600 UTC  
592 then decreasing in the afternoon to less than 50%. Further east in the region including  
593 Brazzaville, Ndjili, Djambala and Souanké (blue, leeward slopes of plateau) the LCOF is  
594 generally lower and shows a stronger diurnal cycle with LCOF varying between 70% in the  
595 morning and 25% in the afternoon (Fig. 11f). Taking the grid point corresponding to each  
596 station, SAFNWC during the day (0600 to 1500 UTC) and NMS at night (1800 to 0300 UTC)  
597 the spatial variability of diurnal cycle is similar to SYNOP observations data (similar ranking  
598 of the groups of stations; Fig. 11g). During the day, we observe an eastward gradient, with a  
599 higher cloud occurrence frequency in the windward slopes and lower cloud cover toward the  
600 inland region (Fig. 11g). At night (0000-0300 UTC) the difference of low-level cloud cover  
601 between the windward slopes and the inland regions is reduced, similarly to SYNOP  
602 observations (Fig. 11f-g). Inconsistencies between SYNOP observations and satellites include  
603 a large underestimation of LCOF at 0600 UTC (see also Fig. 9) and a clear underestimation at  
604 the coastal stations due to less low-level cloud over the ocean in SAFNWC.

605 The reduced low-level cloud cover over the plateau in the afternoon has been previously  
606 associated to the topography favoring a foehn effect (Dommo et al. 2018). The afternoon  
607 clearing occurring on the plateau may also be associated with a shortwave heating and a stronger  
608 convection due to elevated terrain. The development of cumulus in eastern Gabon and central  
609 RC supports this statement (Figure 6). The June-July daytime clearing of the low-level stratus  
610 in southern Benin during the “convective phase”, as described in the conceptual model of  
611 Lohou et al. (2020), provides a potential mechanism in this regard. However, a clear distinction  
612 to the Benin site is the presence of a lush rainforest in Gabon and thus plant transpiration might  
613 be of larger importance. After sunset, the LW cooling of the ground and later of the cloud top  
614 might promote the formation of the clouds.

615 On the windward slopes of southern Cameroon, Equatorial Guinea, Gabon, and RC, the  
616 apparent increase of low-level cloud cover during the morning in the satellites, while collocated  
617 stations do not actually show any LCF increase (Figs. 7 and 11c), may be associated with an  
618 elevation of the boundary layer that make the low-level clouds ‘visible’ to the satellite. Early  
619 in the morning, the low-level cloud top temperature may not be significantly distinct from the  
620 ground temperature, such that the low-level clouds can easily be misclassified as cloud-free by  
621 the satellite’s algorithm. This result suggests a persistence of low-level level clouds as shown  
622 in the SYNOP observations (Fig. 11f) more than a real increase in low-level cloud cover. To  
623 the east of the coastal plains, at the western flank of the low mountain ranges, upslope winds  
624 will support the persistence of clouds. While for West Africa, it was found that advection of  
625 low-level marine stratus onto land plays an inferior role to the extent of the land-based stratus  
626 (Lohou et al., 2020), this may be a contributor south of Port-Gentil where low-level offshore  
627 clouds are frequent and widespread (Fig. 7).

628 Stations directly at the coast, like Port-Gentil at Cape Lopez and Pointe-Noire, but to a  
629 lesser extent Libreville (red stations in Fig. 11e) exhibit a decrease of low-level cloud cover in  
630 the morning, suggesting a frequent land-sea breeze activity, even during the cloudy dry season.  
631 It is interesting to note that the coastal upwelling develops south of Port-Gentil (Herbert and  
632 Bourlès 2018). Thus, the larger ocean-land temperature contrasts at Pointe-Noire and the “cape  
633 location” of Port-Gentil may favor decrease of low-level cloud cover in the morning due to a  
634 sea breeze.

635

#### 636 4. Summary and Discussion

637 In this study, a data set of SYNOP observations of low cloud fraction and low cloud genus  
638 of unprecedented length (1971–2019) and completeness has been compiled for Western  
639 Equatorial Africa. It has been used to provide a climatology of low-level clouds and to evaluate  
640 satellite cloud products, namely SAFNWC and NMS/DMS for the common period JJAS 2008-  
641 2019. SAFNWC, NMS, and DMS products are based on the MSG SEVIRI multi-channel  
642 radiometer and thus have a high spatial (3 km x 3 km) and temporal (15 minutes) resolution.  
643 2B-GEOPROF-LIDAR which is based on the CloudSat CPR and Calipso CALIOP  
644 instruments, and has a low sampling rate (two overflights per day and a return period of 16  
645 days for the same swath), was also considered as it informs on the presence or not, of low-level  
646 clouds in case of a multi-layered cloud cover.

647 Our evaluations of the satellite products (Figure 9) underscore the previously known  
648 deficiencies of SAFNWC at detecting low-level clouds at night in tropical Africa (van der  
649 Linden et al. 2015; Dommo et al. 2018) The lower skill of SAFNWC compared to NMS at  
650 night is demonstrated by the proportion of undetected low-level clouds (all genera): in NMS  
651 only ~25% (Fig. 10h) of the SYNOP low-level clouds are classified in the cloud free category  
652 (among which a significant number of cumulonimbus), whereas in SAFNWC this number is  
653 above 40% (Fig. 10b-c, and comprises mainly stratocumulus). Thresholds used in the NMS  
654 algorithm are probably more efficient to capture low clouds, especially in case of a small  
655 contrast between the ground and the cloud top temperature. A negative bias at night in  
656 SAFNWC due to such a small contrast has previously been reported (van der Linden et al.  
657 2015). Therefore, the use of the NMS, adapted for tropical conditions (Schrage and Fink, 2012)  
658 is also recommended for WEA. Consequently, the concatenation of SAFNWC for daylight  
659 hours (0600–1500 UTC) and NMS for nighttime (1800–0300 UTC) hours yields the most  
660 realistic diurnal cycle compared to SYNOP observations, although caution should be exerted  
661 around sunset and sunrise as both products show large biases. Our study clearly improves on  
662 the results by Dommo et al. (2018) as this former study shows a maximum of low-level cloud  
663 cover in the middle of the day in all parts of WEA, whereas low-level cloud cover (excluding  
664 cumuliform clouds) peaks at late night /early morning.

665 The satellite products SAFNWC and NMS were together able to produce a similar spatial  
666 variability of low-level clouds diurnal cycle compared to SYNOP observations. Mostly, over  
667 the windward slopes of the Cristal and Chaillu mountains (Fig. 1), there is more low-level  
668 clouds all day, while the plateau regions are characterized by a larger amplitude in the diurnal

669 cycle with higher LCOF in the morning, a decrease of LCOF (clearing) in the afternoon, and  
670 low-level clouds that reform late at night (Figs. 7 and 11). However, frequent higher clouds,  
671 making it impossible for most satellite instruments to detect clouds underneath, render the  
672 results more uncertain in the northern part of the study region (i.e. South Cameroon, Fig. 7).  
673 This higher cloud frequency is clear in the 2B-GEOPROF-LIDAR vertical profiles (Fig. 8). It  
674 partly explains the larger underestimation of low-level clouds by SAFNWC and the  
675 microphysical schemes compared to SYNOP observations in this region.

676 Despite uncertainties in both eye observations of clouds at stations and satellite cloud  
677 products, the present study yields the most complete low-level cloud climatology for western  
678 equatorial Africa to date and can provide a basis for further investigations on climate change  
679 aspects of low-level clouds. First, this paper points to the observational and satellite products  
680 that can be used for validating climate models over the historical period for the region. Second,  
681 it documents the mean diurnal evolution of the low-level cloud cover and the spatial variability  
682 of cloud fraction and frequency of occurrence. If models show a good performance at  
683 reproducing these key characteristics over the historical period, then one should have some  
684 confidence to use them for exploring the medium to long-term future evolution of the low-level  
685 cloud cover. Coupled and forced CMIP6 models have still large deficiencies in simulating the  
686 low-level oceanic and continental clouds in the region (Camberlin et al. 2022), but convection-  
687 permitting model simulations, including sensitivity studies, should be suitable to shed more  
688 light on the physical processes involved in the genesis and lysis of the low-level clouds..

#### 689 *Acknowledgements.*

690 The authors thank the reviewers for their time spent on the manuscript and their valuable  
691 comments. We also thank the AERIS/ICARE data center (<http://icare.univ-lille1.fr/>) for  
692 providing access to the SAFNWC CT data used in this study. This study was part of the project  
693 DYVALOCCA (<https://dyvalocca.osug.fr/>) funded by

694 ANR and DFG under Contract ANR-19-CE01-0021 and DFG FI 786/5-1

#### 695 *Data availability statement.*

696 The datasets used to create the concatenated SYNOP dataset are from different sources :  
697 EECRA is available at <https://rda.ucar.edu/datasets/ds292.2/#access>  
698 ISD is from [https://www.ncei.noaa.gov/products/land-based-station/integrated-surface-](https://www.ncei.noaa.gov/products/land-based-station/integrated-surface-database)  
699 [database.](https://www.ncei.noaa.gov/products/land-based-station/integrated-surface-database)

700 MIDAS is from <https://catalogue.ceda.ac.uk/uuid/220a65615218d5c9cc9e4785a3234bd0>.  
701 SAFNWC is available upon request from the AERIS/ICARE data center (<http://icare.univ-lille1.fr/>).  
702  
703 DMS/NMS can be downloaded here  
704 <https://data.eumetsat.int/product/EO:EUM:DAT:MSG:HRSEVIRI#>.  
705 2B-GEOPROF-LIDAR is available here: [2B-GEOPROF-LIDAR | CloudSat DPC](#)  
706 ([colostate.edu](http://colostate.edu))  
707 The concatenated SYNOP observations dataset and the low cloud occurrence frequency and  
708 low cloud fraction from SAFNWC, NMS/DMS and 2B-GEOPROF-LIDAR produced in this  
709 study are available upon request.

710

## 711 REFERENCES

- 712 Adebisi, A. A., and P. Zuidema, 2018: Low Cloud Cover Sensitivity to Biomass-Burning  
713 Aerosols and Meteorology over the Southeast Atlantic. *J. Clim.*, **31**, 4329–4346,  
714 <https://doi.org/10.1175/JCLI-D-17-0406.1>.
- 715 Aellig, R., V. Moron, and P. Camberlin, 2022: Cloud observing data of 85 stations in western  
716 Central Africa. <https://doi.org/10.5445/IR/1000150635>.
- 717 Andersen, H., and J. Cermak, 2018: First fully diurnal fog and low cloud satellite detection  
718 reveals life cycle in the Namib. *Atmospheric Meas. Tech.*, **11**, 5461–5470,  
719 <https://doi.org/10.5194/amt-11-5461-2018>.
- 720 ———, ———, I. Solodovnik, L. Lelli, and R. Vogt, 2019: Spatiotemporal dynamics of fog and  
721 low clouds in the Namib unveiled with ground- and space-based observations.  
722 *Atmospheric Chem. Phys.*, **19**, 4383–4392, <https://doi.org/10.5194/acp-19-4383-2019>.
- 723 ———, ———, J. Fuchs, P. Knippertz, M. Gaetani, J. Quinting, S. Sippel, and R. Vogt, 2020:  
724 Synoptic-scale controls of fog and low-cloud variability in the Namib Desert.  
725 *Atmospheric Chem. Phys.*, **20**, 3415–3438, <https://doi.org/10.5194/acp-20-3415-2020>.
- 726 Bayon, G., and Coauthors, 2019: The roles of climate and human land-use in the late  
727 Holocene rainforest crisis of Central Africa. *Earth Planet. Sci. Lett.*, **505**, 30–41,  
728 <https://doi.org/10.1016/j.epsl.2018.10.016>.
- 729 Berry, Z. C., and G. R. Goldsmith, 2020: Diffuse light and wetting differentially affect  
730 tropical tree leaf photosynthesis. *New Phytol.*, **225**, 143–153,  
731 <https://doi.org/10.1111/nph.16121>.
- 732 Burnett, M. W., G. R. Quetin, and A. G. Konings, 2020: Data-driven estimates of  
733 evapotranspiration and its controls in the Congo Basin. *Hydrol. Earth Syst. Sci.*, **24**,  
734 4189–4211, <https://doi.org/10.5194/hess-24-4189-2020>.
- 735 Bush, E. R., and Coauthors, 2020: Rare ground data confirm significant warming and drying  
736 in western equatorial Africa. *PeerJ*, **8**, e8732, <https://doi.org/10.7717/peerj.8732>.



- 737 Camberlin, P., and Coauthors, 2022: The Representation of Dry-Season Low-Level Clouds  
738 Over Western Equatorial Africa in Reanalyses and Historical CMIP6 Simulations.  
739 *Submitted to Climate Dynamics*.
- 740 Danielson, J. J., and D. B. Gesch, 2011: *Global multi-resolution terrain elevation data 2010*  
741 (*GMTED2010*). U.S. Geological Survey Open-File Report,.
- 742 Dee, D. P., and Coauthors, 2011: The ERA-Interim reanalysis: configuration and  
743 performance of the data assimilation system. *Q. J. R. Meteorol. Soc.*, **137**, 553–597,  
744 <https://doi.org/10.1002/qj.828>.
- 745 Derrien, M., and H. Le Gléau, 2005: MSG/SEVIRI cloud mask and type from SAFNWC. *Int.*  
746 *J. Remote Sens.*, **26**, 4707–4732, <https://doi.org/10.1080/01431160500166128>.
- 747 ———, H. L. Gleau, and P. Fernandez, 2013: *Algorithm Theoretical Basis Document for*  
748 *“Cloud Products” (CMa-PGE01 v3.2, CT-PGE02 v2.2 & CTTH-PGE03 v2.2)*.  
749 [https://www.nwcsaf.org/AemetWebContents/ScientificDocumentation/Documentatio](https://www.nwcsaf.org/AemetWebContents/ScientificDocumentation/Documentation/MSG/SAF-NWC-CDOP2-MFL-SCI-ATBD-01_v3.2.1.pdf)  
750 [n/MSG/SAF-NWC-CDOP2-MFL-SCI-ATBD-01\\_v3.2.1.pdf](https://www.nwcsaf.org/AemetWebContents/ScientificDocumentation/Documentation/MSG/SAF-NWC-CDOP2-MFL-SCI-ATBD-01_v3.2.1.pdf).
- 751 Dommo, A., N. Philippon, D. A. Vondou, G. Sèze, and R. Eastman, 2018: The June–  
752 September Low Cloud Cover in Western Central Africa: Mean Spatial Distribution  
753 and Diurnal Evolution, and Associated Atmospheric Dynamics. *J. Clim.*, **31**, 9585–  
754 9603, <https://doi.org/10.1175/JCLI-D-17-0082.1>.
- 755 Eastman, R., and S. G. Warren, 2014: Diurnal Cycles of Cumulus, Cumulonimbus, Stratus,  
756 Stratocumulus, and Fog from Surface Observations over Land and Ocean. *J. Clim.*,  
757 **27**, 2386–2404, <https://doi.org/10.1175/JCLI-D-13-00352.1>.
- 758 EUMeTrain, 2017: Composite Image Quick Guide.  
759 [http://eumetrain.org/rgb\\_quick\\_guides/index.html](http://eumetrain.org/rgb_quick_guides/index.html) (Accessed April 14, 2022).
- 760 Fleury, L., and Coauthors, 2011: AMMA information system: an efficient cross-disciplinary  
761 tool and a legacy for forthcoming projects. *Atmospheric Sci. Lett.*, **12**, 149–154,  
762 <https://doi.org/10.1002/asl.303>.
- 763 Fuchs, J., J. Cermak, and H. Andersen, 2018: Building a cloud in the southeast Atlantic:  
764 understanding low-cloud controls based on satellite observations with machine  
765 learning. *Atmospheric Chem. Phys.*, **18**, 16537–16552, [https://doi.org/10.5194/acp-18-](https://doi.org/10.5194/acp-18-16537-2018)  
766 [16537-2018](https://doi.org/10.5194/acp-18-16537-2018).
- 767 Geleyn, J.-F., and A. Hollingsworth, 1979: An economical analytical method for the  
768 computation of the interaction between scattering and line absorption of radiation.  
769 *Beitr Phys Atmos*, **52**, 1–16.
- 770 Goldsmith, G. R., N. J. Matzke, and T. E. Dawson, 2013: The incidence and implications of  
771 clouds for cloud forest plant water relations. *Ecol. Lett.*, **16**, 307–314,  
772 <https://doi.org/10.1111/ele.12039>.
- 773 Hahn, C., S. Warren, and R. Eastman, 1999: Extended Edited Synoptic Cloud Reports from  
774 Ships and Land Stations Over the Globe, 1952–2009 (NDP-026C).  
775 <https://doi.org/10.3334/CDIAC/CLI.NDP026C>.
- 776 Herbert, G., and B. Bourlès, 2018: Impact of intraseasonal wind bursts on sea surface  
777 temperature variability in the far eastern tropical Atlantic Ocean during boreal spring  
778 2005 and 2006: focus on the mid-May 2005 event. *Ocean Sci.*, **14**, 849–869,  
779 <https://doi.org/10.5194/os-14-849-2018>.
- 780 Hu, Z.-Z., B. Huang, and K. Pegion, 2008: Low cloud errors over the southeastern Atlantic in

- 781 the NCEP CFS and their association with lower-tropospheric stability and air-sea  
782 interaction. *J. Geophys. Res.*, **113**, D12114, <https://doi.org/10.1029/2007JD009514>.
- 783 Kalthoff, N., and Coauthors, 2018: An overview of the diurnal cycle of the atmospheric  
784 boundary layer during the West African monsoon season: results from the 2016  
785 observational campaign. *Atmospheric Chem. Phys.*, **18**, 2913–2928,  
786 <https://doi.org/10.5194/acp-18-2913-2018>.
- 787 Karger, D. N., M. Kessler, M. Lehnert, and W. Jetz, 2021: Limited protection and ongoing  
788 loss of tropical cloud forest biodiversity and ecosystems worldwide. *Nat. Ecol. Evol.*,  
789 **5**, 854–862, <https://doi.org/10.1038/s41559-021-01450-y>.
- 790 Knippertz, P., A. H. Fink, R. Schuster, J. Trentmann, J. M. Schrage, and C. Yorke, 2011:  
791 Ultra-low clouds over the southern West African monsoon region: ULTRA-LOW  
792 CLOUDS OVER WEST AFRICA. *Geophys. Res. Lett.*, **38**, n/a-n/a,  
793 <https://doi.org/10.1029/2011GL049278>.
- 794 ———, and Coauthors, 2015: The DACCIWA Project: Dynamics–Aerosol–Chemistry–Cloud  
795 Interactions in West Africa. *Bull. Am. Meteorol. Soc.*, **96**, 1451–1460,  
796 <https://doi.org/10.1175/BAMS-D-14-00108.1>.
- 797 Lensky, I. M., and D. Rosenfeld, 2008: Clouds-Aerosols-Precipitation Satellite Analysis Tool  
798 (CAPSAT). *Atmospheric Chem. Phys.*, **8**, 6739–6753, <https://doi.org/10.5194/acp-8-6739-2008>.
- 800 van der Linden, R., A. H. Fink, and R. Redl, 2015: Satellite-based climatology of low-level  
801 continental clouds in southern West Africa during the summer monsoon season: Low-  
802 level clouds in southern West Africa. *J. Geophys. Res. Atmospheres*, **120**, 1186–1201,  
803 <https://doi.org/10.1002/2014JD022614>.
- 804 Lohou, F., N. Kalthoff, B. Adler, K. Babić, C. Dione, M. Lothon, X. Pedruzo-Bagazgoitia,  
805 and M. Zouzoua, 2020: Conceptual model of diurnal cycle of low-level stratiform  
806 clouds over southern West Africa. *Atmospheric Chem. Phys.*, **20**, 2263–2275,  
807 <https://doi.org/10.5194/acp-20-2263-2020>.
- 808 Mace, G. G., and Q. Zhang, 2014: The CloudSat radar-lidar geometrical profile product (RL-  
809 GeoProf): Updates, improvements, and selected results: CLOUDSAT RADAR-  
810 LIDAR GEOMETRICAL PROFILE. *J. Geophys. Res. Atmospheres*, **119**, 9441–9462,  
811 <https://doi.org/10.1002/2013JD021374>.
- 812 ———, ———, M. Vaughan, R. Marchand, G. Stephens, C. Trepte, and D. Winker, 2009: A  
813 description of hydrometeor layer occurrence statistics derived from the first year of  
814 merged Cloudsat and CALIPSO data. *J. Geophys. Res.*, **114**, D00A26,  
815 <https://doi.org/10.1029/2007JD009755>.
- 816 Maley, J., and E. Hilaire, 1993: The role of clouds in the evolution of tropical African  
817 palaeoenvironments. *Veille climatique satellitaire*. **46**, 51–63.
- 818 Mallet, M., P. Nabat, B. Johnson, M. Michou, J. M. Haywood, C. Chen, and O. Dubovik,  
819 2021: Climate models generally underrepresent the warming by Central Africa  
820 biomass-burning aerosols over the Southeast Atlantic. *Sci. Adv.*, **7**, eabg9998,  
821 <https://doi.org/10.1126/sciadv.abg9998>.
- 822 Marchand, R., G. G. Mace, T. Ackerman, and G. Stephens, 2008: Hydrometeor Detection  
823 Using Cloudsat—An Earth-Orbiting 94-GHz Cloud Radar. *J. Atmospheric Ocean.  
824 Technol.*, **25**, 519–533, <https://doi.org/10.1175/2007JTECHA1006.1>.

- 825 Met Office, 2012: Met Office Integrated Data Archive System (MIDAS) Land and Marine  
826 Surface Stations Data (1853-current).  
827 <https://catalogue.ceda.ac.uk/uuid/220a65615218d5c9cc9e4785a3234bd0>.
- 828 Oliveira, R. S., C. B. Eller, P. R. L. Bittencourt, and M. Mulligan, 2014: The hydroclimatic  
829 and ecophysiological basis of cloud forest distributions under current and projected  
830 climates. *Ann. Bot.*, **113**, 909–920, <https://doi.org/10.1093/aob/mcu060>.
- 831 Painemal, D., K.-M. Xu, A. Cheng, P. Minnis, and R. Palikonda, 2015: Mean Structure and  
832 Diurnal Cycle of Southeast Atlantic Boundary Layer Clouds: Insights from Satellite  
833 Observations and Multiscale Modeling Framework Simulations. *J. Clim.*, **28**, 324–  
834 341, <https://doi.org/10.1175/JCLI-D-14-00368.1>.
- 835 Philippon, N., and Coauthors, 2019: The light-deficient climates of western Central African  
836 evergreen forests. *Environ. Res. Lett.*, **14**, 034007, <https://doi.org/10.1088/1748-9326/aaf5d8>.
- 838 Philippon, N., A. Ouhechou, P. Camberlin, J. Trentmann, A. H. Fink, J. D. Maloba, B. Morel,  
839 and G. Samba, 2022: Characterization of Sunshine Duration in Western Equatorial  
840 Africa: In Situ Measurements versus SARA-2 Satellite Estimates. *J. Appl. Meteorol.*  
841 *Climatol.*, **61**, 185–201.
- 842 Räisänen, P., H. W. Barker, M. F. Khairoutdinov, J. Li, and D. A. Randall, 2004: Stochastic  
843 generation of subgrid-scale cloudy columns for large-scale models. *Q. J. R. Meteorol.*  
844 *Soc.*, **130**, 2047–2067, <https://doi.org/10.1256/qj.03.99>.
- 845 Schmetz, J., P. Pili, S. Tjemkes, D. Just, J. Kerkmann, S. Rota, and A. Ratier, 2002: An  
846 Introduction to Meteosat Second Generation (MSG). *Bull. Am. Meteorol. Soc.*, **83**,  
847 992–992, <https://doi.org/10.1175/BAMS-83-7-Schmetz-2>.
- 848 Schrage, J. M., and A. H. Fink, 2012: Nocturnal Continental Low-Level Stratus over Tropical  
849 West Africa: Observations and Possible Mechanisms Controlling Its Onset. *Mon.*  
850 *Weather Rev.*, **140**, 1794–1809, <https://doi.org/10.1175/MWR-D-11-00172.1>.
- 851 Schuster, R., A. H. Fink, and P. Knippertz, 2013: Formation and Maintenance of Nocturnal  
852 Low-Level Stratus over the Southern West African Monsoon Region during AMMA  
853 2006. *J. Atmospheric Sci.*, **70**, 2337–2355, <https://doi.org/10.1175/JAS-D-12-0241.1>.
- 854 Smith, A., N. Lott, and R. Vose, 2011: The Integrated Surface Database: Recent  
855 Developments and Partnerships. *Bull. Am. Meteorol. Soc.*, **92**, 704–708,  
856 <https://doi.org/10.1175/2011BAMS3015.1>.
- 857 Solmon, F., N. Elguindi, M. Mallet, C. Flamant, and P. Formenti, 2021: West African  
858 monsoon precipitation impacted by the South Eastern Atlantic biomass burning  
859 aerosol outflow. *Npj Clim. Atmospheric Sci.*, **4**, 54, <https://doi.org/10.1038/s41612-021-00210-w>.
- 861 Stephens, G. L., and Coauthors, 2002: THE CLOUDSAT MISSION AND THE A-TRAIN:  
862 A New Dimension of Space-Based Observations of Clouds and Precipitation. *Bull.*  
863 *Am. Meteorol. Soc.*, **83**, 1771–1790, <https://doi.org/10.1175/BAMS-83-12-1771>.
- 864 Wilson, A. M., and W. Jetz, 2016: Remotely Sensed High-Resolution Global Cloud  
865 Dynamics for Predicting Ecosystem and Biodiversity Distributions. *PLOS Biol.*, **14**,  
866 e1002415, <https://doi.org/10.1371/journal.pbio.1002415>.
- 867 Winker, D. M., J. R. Pelon, and M. P. McCormick, 2003: The CALIPSO mission: spaceborne  
868 lidar for observation of aerosols and clouds. U.N. Singh, T. Itabe, and Z. Liu, Eds.,

- 869 Third International Asia-Pacific Environmental Remote Sensing Remote Sensing of  
870 the Atmosphere, Ocean, Environment, and Space, Hangzhou, China, 1.
- 871 WMO, 2019: Identifying the genus | International Cloud Atlas.  
872 <https://cloudatlas.wmo.int/en/identifying-the-genus.html> (Accessed October 21,  
873 2021).
- 874 Wood, R., 2012: Stratocumulus Clouds. *Mon. Weather Rev.*, **140**, 2373–2423,  
875 <https://doi.org/10.1175/MWR-D-11-00121.1>.